AD-A179 665 APPLICATION OF ATOMIC FLUORESCENCE TO MEASUREMENT OF COMBUSTION TEMPERATU..(U) SYSTEMS RESEARCH LABS INC DAYTON OH L P GOSS ET AL. 04 DEC 86 SRL-6009 1/1

UNCLASSIFIED AFOSR-TR-87-0565 F49620-83-C-0130 F/G 21/9.2 NL

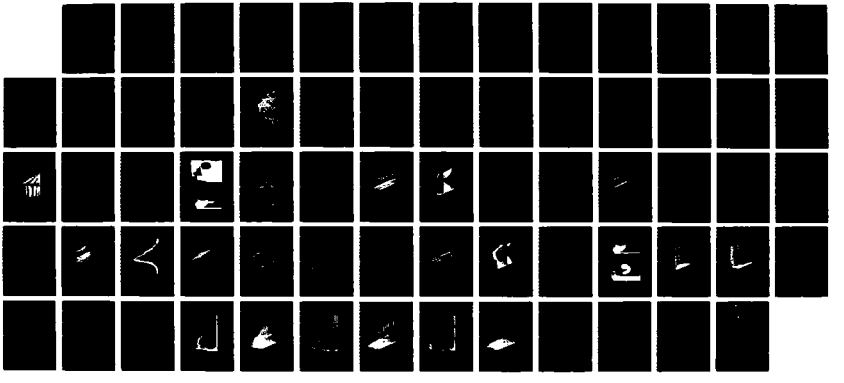

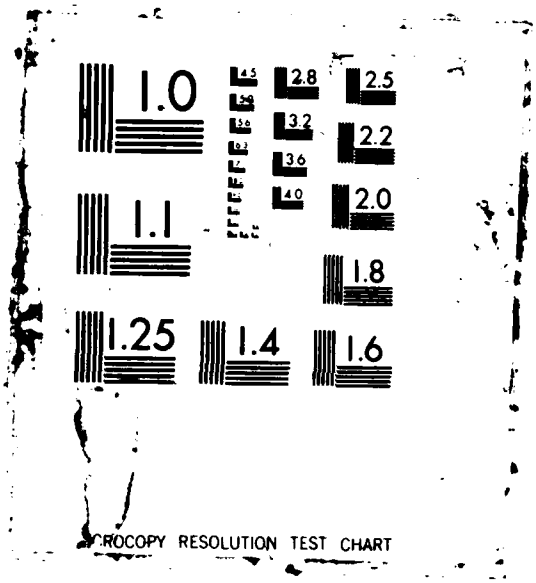
1.0
1.1
1.25
1.4
1.6
2.8
3.2
3.6
4.0
2.5
2.2
2.0
1.8
ROCOPY RESOLUTION TEST CHART

UNCLASSIFIED

AD-A179 665

DTIC FILE COPY (2)

REPORT DOCUMENTATION PAGE

1a. REPORT SECURITY CLASSIFICATION: Unclassified	1b. RESTRICTIVE MARKINGS:
2a. SECURITY CLASSIFICATION AUTHORITY:	3. DISTRIBUTION/AVAILABILITY OF REPORT: Approved for public release; distribution unlimited.
2b. DECLASSIFICATION/DOWNGRADING SCHEDULE:	
4. PERFORMING ORGANIZATION REPORT NUMBER(S): 6809 Final	5. MONITORING ORGANIZATION REPORT NUMBER(S): AFOSR-TR- 87-0565
6a. NAME OF PERFORMING ORGANIZATION: Systems Research Laboratories, Inc. / 6b. OFFICE SYMBOL (If applicable):	7a. NAME OF MONITORING ORGANIZATION: U. S. Air Force Office of Scientific Research
6c. ADDRESS (City, State and ZIP Code): 2800 Indian Ripple Road Dayton, OH 45440-3696	7b. ADDRESS (City, State and ZIP Code): AFOSR/NA, Bldg 410 Bolling AFB, D. C. 20332-6448
8a. NAME OF FUNDING/SPONSORING ORGANIZATION: U. S. Air Force Office of Scientific Research / 8b. OFFICE SYMBOL (If applicable): AFOSR/NA	9. PROCUREMENT INSTRUMENT IDENTIFICATION NUMBER: F49620-83-C-0138
8c. ADDRESS (City, State and ZIP Code): Bolling AFB, D. C. 20332-6448 Bldg 410	10. SOURCE OF FUNDING NOS.

PROGRAM ELEMENT NO.	PROJECT NO.	TASK NO.	WORK UNIT NO.
61102F	2308	A3	

11. TITLE (Include Security Classification): Application of Atomic Fluorescence to Measurement of Combustion Temperature in Solid Propellants

12. PERSONAL AUTHOR(S): L. P. Goss, Ph.D., and A. A. Smith

13a. TYPE OF REPORT	13b. TIME COVERED	14. DATE OF REPORT (Yr., Mo., Day)	15. PAGE COUNT
Final	FROM 84-8-1 TO 86-7-31	86-12-4	66

16. SUPPLEMENTARY NOTATION

17. COSATI CODES		
FIELD	GROUP	SUB. GR.
21	09.2	
06	05	

18. SUBJECT TERMS (Continue on reverse if necessary and identify by block number): Surface Temperature, Laser-Induced Fluorescence, Thermography, Solid ~~Fuel~~ rocket Propellants, Rare-Earth Ions, ~~Single-Shot~~ Thermography, Nonintrusive Optical Diagnostics, (Continued)

19. ABSTRACT (Continue on reverse if necessary and identify by block number)

A method has been developed for nonintrusive collection of surface-temperature data from reactive and nonreactive surfaces. The method relies on the temperature sensitivity of the laser-induced fluorescence of a rare-earth ion which has been seeded into the material under study. The rare-earth ion (dysprosium) doped into a crystal (yttrium-aluminum-garnet) is shown to be an ideal seed, the fluorescence of which is stimulated by the ultraviolet output of a Nd:YAG laser. The fluorescence of the crystal is collected by a linear-array detector, analyzed, and stored for evaluation. Calibration of this method has been made from 300 to 1673 K. Tests have been conducted on reactive and nonreactive surfaces. Additionally, a technique for obtaining temperature depth profiles of reactive materials has been developed, and test results are shown. (keywords:)

DTIC ELECTE APR 27 1987 E

20. DISTRIBUTION/AVAILABILITY OF ABSTRACT	21. ABSTRACT SECURITY CLASSIFICATION
UNCLASSIFIED/UNLIMITED ☒ SAME AS RPT. ☐ DTIC USERS ☐	Unclassified

22a. NAME OF RESPONSIBLE INDIVIDUAL	22b. TELEPHONE NUMBER (Include Area Code)	22c. OFFICE SYMBOL
Julian Tishkoff, Ph.D.	(202) 767-4935	AFOSR/NA

DD FORM 1473, 83 APR — EDITION OF 1 JAN 73 IS OBSOLETE.

UNCLASSIFIED

SECURITY CLASSIFICATION OF THIS PAGE

Block 18. SUBJECT TERMS (Continued)

Thermographic Imaging, Temperature Depth Profiling, High Spatial Resolution, High Temporal Resolution, Reactive ~~and Nonreactive~~ Surfaces

Preface

This report was prepared by Larry P. Goss, Ph.D., and Arthur A. Smith and covers work performed during the period 1 August 1984 through 31 July 1986 under Air Force Office of Scientific Research Contract No. F49620-83-C-0138. The AFOSR contract monitor was Julian Tishkoff, Ph.D.

TABLE OF CONTENTS

LIST OF ILLUSTRATIONS

LIST OF ILLUSTRATIONS (Continued)

LIST OF ILLUSTRATIONS (Concluded)

Nomenclature

C_c = Specific heat of crystal

C_p = Specific heat of particle

d_c = Diameter of crystal

E_s = Activation energy at burning surface

f = Frequency

f_c = Cutoff frequency

I_f = Thermal feedback from flame

K = Thermal conductivity

k_p = Thermal conductivity of particle

Q = Radiation flux

R = Ideal gas constant

r = Burn rate

T = Surrounding temperature

T_c = Crystal temperature

T_f = Flame temperature

T_o = Initial temperature

T_s = Surface temperature

U_s = Velocity of surrounding gases

z_s = Pre-exponential factor

λ_g = Thermal constant of gas

λ_p = Thermal constant of propellant

λ_T = Thermal wavelength

ρ_c = Crystal density

ρ_p = Particle density

ρ_s = Surface density

τ = Crystal time constant

Section 1

INTRODUCTION

This report describes experimental and theoretical investigations of laser-induced fluorescence as a diagnostic technique for remotely determining the temperature of reacting and nonreacting surfaces.

Condensed-phase combustion processes of energetic materials in intermediate- (3 - 20 MPa) and high- (> 300 mPa) pressure regions present many challenges for researchers in the field of optical diagnostics; to date, this area has received less attention than the experimentally more-tractable problem of gas-phase combustion. The choice of a diagnostic technique for surface-temperature measurements is complicated by the requirements of high spatial resolution (1 μm), high temporal resolution (> 1μs), nonintrusiveness, remote μrobing, and making measurements on an ever-changing reacting surface.

The need to measure the surface and near-surface temperatures of energetic materials can be more fully understood by examining the burning process of such materials. Propellants produce heat and high-temperature gases through the phenomenon of combustion. The thermal feedback from the high-temperature gases to the unburned portion of the propellant raises the propellant to the decomposition temperature. As a result, the unburned portion gasifies and produces heat by an exothermic chemical reaction. The thermal-feedback process sustains propellant burning.

Figure 1 is a schematic of a one-dimensional combustion-wave structure of a solid propellant.[1] The temperature increases rapidly from the initial temperature T_0 to the temperature T_s at the burning surface. At the burning surface, either an endothermic or exothermic decomposition reaction produces reactive gases. This region is called the surface-phase-reaction or condensed-phase-reaction zone. The reactive gases are emitted from the burning surface and generate heat to form a luminous flame zone.

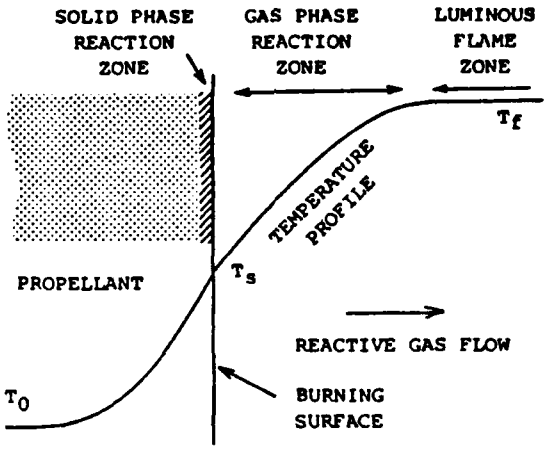

Figure 1. One-Dimensional Combustion-Wave Structure of Solid Propellant (from Ref. 1).

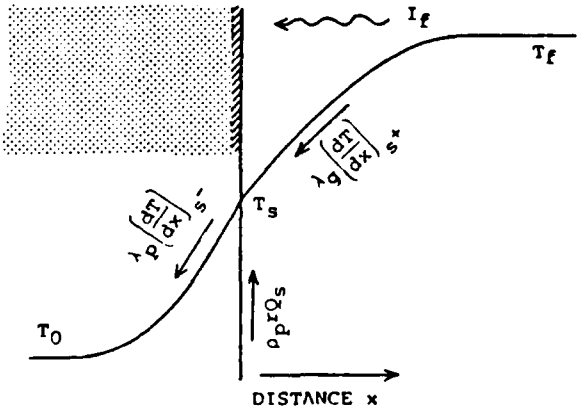

Figure 2. Heat Balance at Burning Surface of Steadily Burning Propellant (from Ref. 1).

The combustion products flow continuously downstream from the combustion zone, and the burning surface recedes in the direction opposite that of the combustion-product flow. The thermal-feedback process due to combustion[1] is shown in Fig. 2. The heat buildup at the surface is a balance of the heat loss to the bulk material and the heat produced by the surface reaction and the surrounding luminous gases. Surface temperature is, thus, a direct indicator of burning rate and can be related by an Arrhenius-type pyrolysis law

$$r = z_s \exp(- E_s/RT_s) \qquad (1)$$

where E_s is the activation energy at the burning surface and z_s is the pre-exponential factor.

Figures 1 and 2 are for idealized one-dimensional propellants where multi-dimensional effects are not considered. In such a case a thin-wire-thermocouple measurement can be used to characterize the temperature profile of the propellant. In practical propellants this is far from the case. In real propellants the temperature profile over the surface is nonuniform, indicating a nonuniform burning rate. Thus, a detailed understanding of propellant combustion and transient effects requires two-dimensional measurements of the surface temperature.

Advanced optical diagnostics such as coherent anti-Stokes Raman spectroscopy (CARS), ordinary Raman spectroscopy, and laser-induced fluorescence (LIF) have been employed extensively for combustion measurements in atmospheric flames and plumes of energetic materials.[2] However, no attempt has been made to apply these techniques to the measurement of reacting surface temperatures. Of the available optical diagnostic techniques, LIF was considered by the authors to hold the most promise of meeting the criteria for an effective diagnostic method for surface-temperature measurements. However, to the authors' knowledge, no molecular or atomic species exists naturally in the propellants which can be used for LIF surface-temperature measurements. Thus, for this technique to be employed, it was necessary to introduce into the

energetic material a fluorescent species whose emission spectrum displayed sensitivity to temperature over the temperature range of interest.

Atomic species such as indium and thallium which have low-lying electronic states populated at relatively low temperatures have been successfully employed in atmospheric flames for making thermometric measurements. However, because of the amorphous nature of energetic materials, the atomic fluorescence is either quenched or homogeneously broadened to the point where it cannot be detected. Attention was thus directed from the conventional atomic species to species such as rare-earth ions which are known to fluoresce in the solid state and be quite sensitive to temperature changes. Since rare-earth ions are not conventional dopant species for thermometry, their temperature sensitivity will be discussed (see Section 3).

This report will discuss the calibration and temporal response of the rare-earth dopants along with their utilization for surface thermographic imaging of nonreacting and reacting surfaces. A novel approach for obtaining temperature depth profiles is also demonstrated.

Section 2

OBJECTIVES

2.1 Introduction

The overall aim of this program was to develop a diagnostic technique capable of measuring the temperature of reactive surfaces undergoing combustion processes. The primary goal was to demonstrate that laser-induced fluorescence (LIF) of embedded seed particles could be used to monitor the surface-temperature profile of a solid undergoing very rapid heating. This was to be accomplisehd by selecting a model material, doping it with the temperature-sensitive seed, and subjecting it to high-energy flux from a CW CO_2 laser.

2.2 Experimental Approach

In order to utilize LIF in this study, three experimental objectives had to be met. The first involved selection of a proper dopant which could be incorporated into the reacting material. The second was to calibrate and verify that the dopant could, in fact, yield the correct surface temperatures. The third objective was actual application of the LIF technique to the determination of surface temperatures of model materials under very rapid CO_2 laser heating.

The three objectives of this program have been accomplished and are discussed in this report. Personnel connected with fulfillment of this contract are as follows:

Co-Principal Investigator:	L. P. Goss, Ph.D.
Co-Principal Investigator:	A. A. Smith, Research Physicist
Physical Science Technician:	M. Rowe

Section 3

LABORATORY STUDIES

3.1 Temperature Sensitivity

Temperature may affect the spectrum of rare-earth ions in several ways. First, the addition of heat causes the crystal lattice containing the rare earth to vibrate which, in turn, creates a changing crystal field at the location of the rare-earth ion and produces a broadening in the linewidth of the optical transitions. Secondly, as the temperature is increased, the number of upper levels of the system which become populated increases according to Boltzmann's law: $\exp(-\Delta\varepsilon/kT)$. This "thermalization" effect causes a change in the intensity distribution of the rare-earth spectrum with temperature. Thirdly, a frequency shift of the spectral lines can occur due to the thermal expansion of the crystal lattice. The greater average ion separation at high temperature results in a reduced crystal field and, in turn, reduced Stark-component separation. Finally, as the temperature increases, the vibration of the crystal lattice (phonons) nonradiatively relaxes the excited electronic state, thus reducing the lifetime of the radiative transition (quenching). Of these effects, the "thermalization" process has been shown to be the optimum technique for surface thermometry.

The "thermalization" process of these compounds can be explained by the small spacing of their energy levels. When two rare-earth energy levels are separated by $< 1000\ cm^{-1}$, the upper level typically will not fluoresce at low temperature due to extremely high multi-phonon relaxation rates which act to quench these closely spaced levels. Thus, at low temperatures, no population buildup occurs in the upper energy level and, therefore, no fluorescence is observed. As the temperature increases, the upper level becomes more populated and the fluorescence from this level increases. Thus, by monitoring the increase in fluorescence of the upper level relative to the lower, the temperature can be determined.

An example of this type of behavior is found in trivalent dysprosium, doped at 3% in yttrium-aluminum-garnet (Dy^{+3}:YAG) (simplified energy diagram shown in Fig. 3). Absorbed laser light excites Dy^{+3} into a high-energy state which radiatively and nonradiatively decays to the F-level. This level undergoes a fast thermal equilibrium which pumps a portion of its population into the nearby G-level. The fluorescence is then observed from both states. Figure 4 displays the fluorescence from both the F- and G-levels of Dy:YAG, including various Stark-shifted components as a function of temperature. The relative intensity of the F-fluorescent level located at 496 nm remains fixed as the temperature increases, while the intensity of the G-level component located at 467 nm increases dramatically with temperature.

It is evident from Fig. 4 that several regions of the Dy:YAG spectrum are temperature sensitive and can be used for thermometry. It is also evident that the 496-nm peak can be used for an internal standard which allows the temperature determination to be a relative measurement rather than a more-difficult absolute measurement. The ratios of the 448-, 456-, 467-, and 512-nm peaks relative to the 496-nm peak are shown in Figs. 5 - 8. The ratios of the peaks which are blue in wavelength display similar behavior to the 496-nm peak, with an S-type curve showing high-temperature sensitivity up to 1800 K. Above this value the fluorescence intensity drops below detectable limits. The 512-nm peak ratio is different in that it is insensitive to temperatures below 500 K but then rapidly increases in sensitivity at high temperatures.

The fluorescence from the G- and F-levels of Dy:YAG extinguishes at a temperature of $\sim$ 1800 K due to the large phonon quenching rates at this high temperature; the melting temperature of the YAG crystal is $\sim$ 2100 K. This operating range is more than adequate for monitoring surface temperatures on energetic materials.

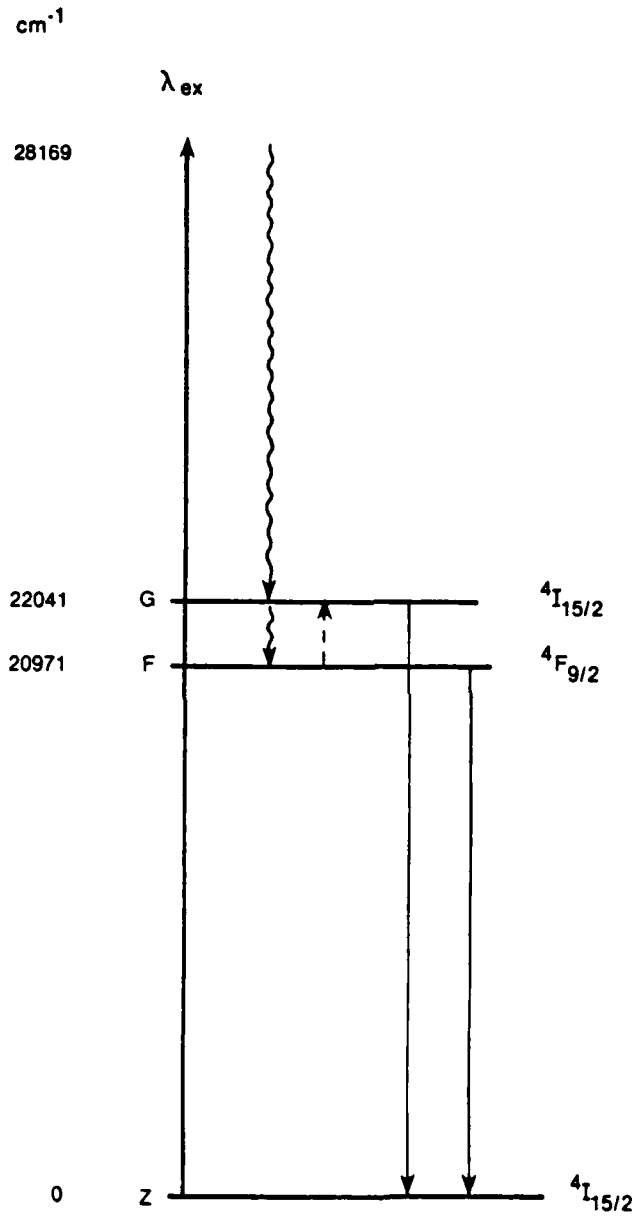

Figure 3. Simplified Energy Diagram of F- and G-Levels of Dy:YAG.

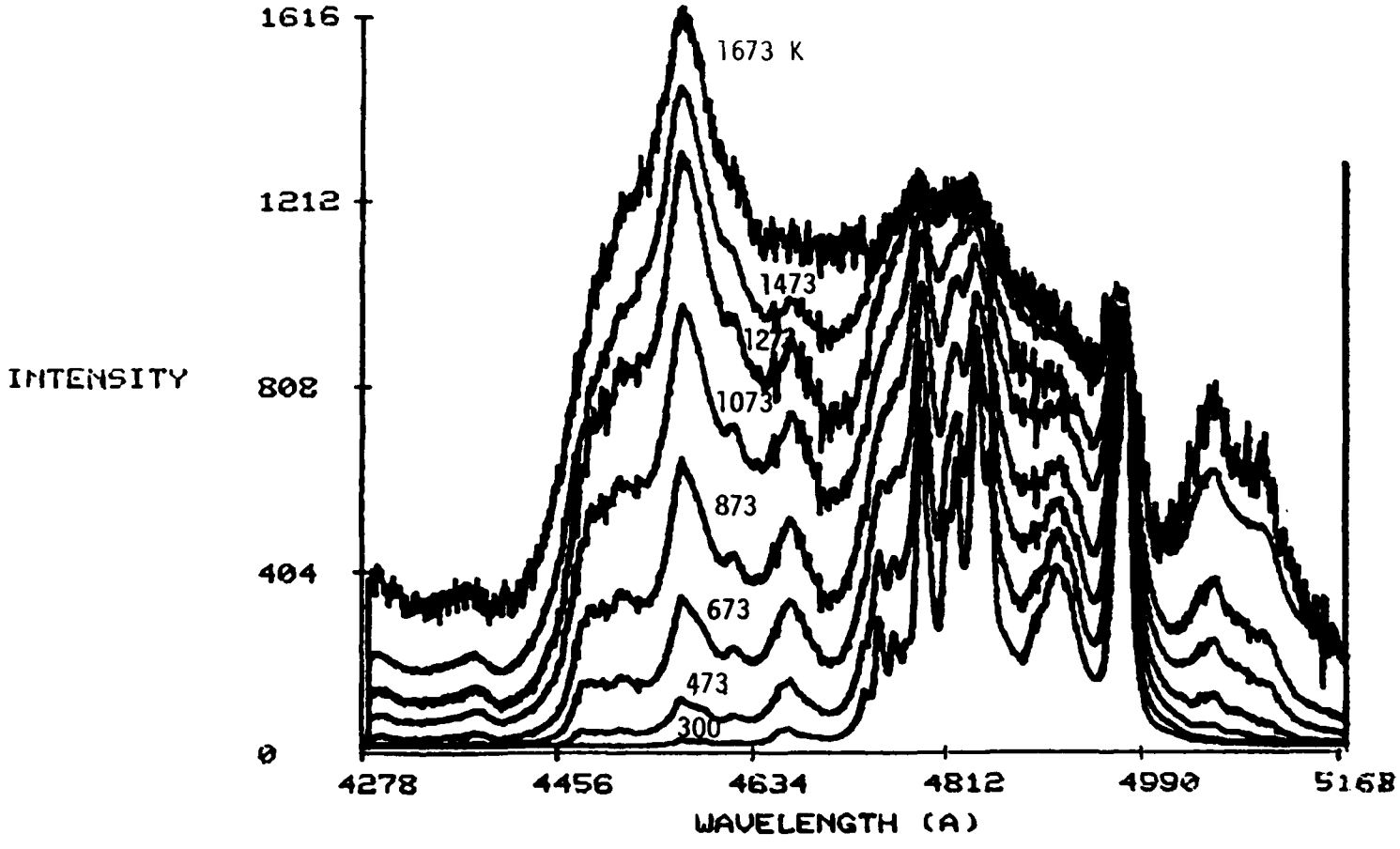

Figure 4. Fluorescence of F- and G-Levels of Dy:YAG as Function of Temperature.

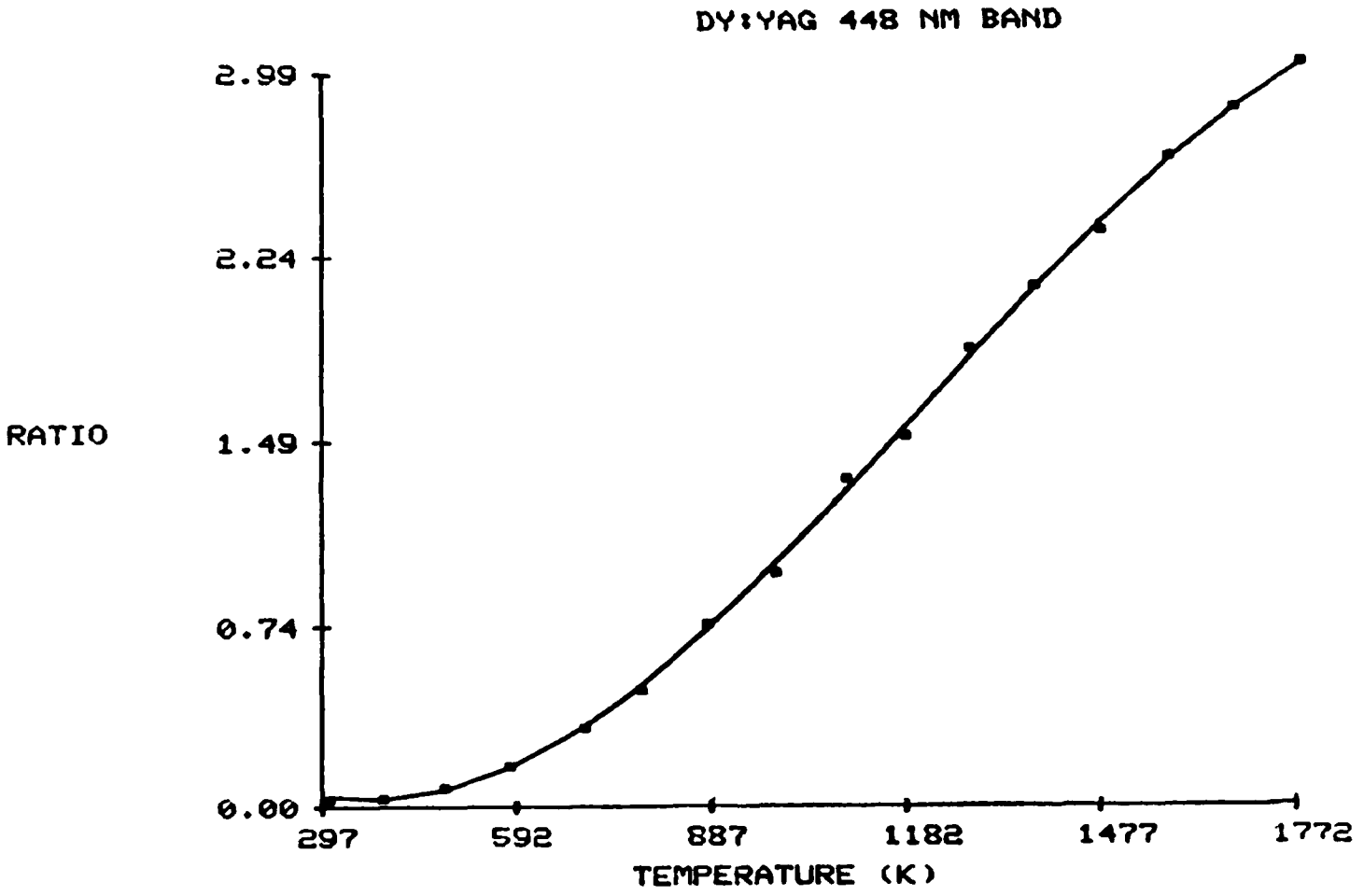

Figure 5. Variation of Relative Intensity of 448-nm G-Level Stark Component to 496-nm F-Level of Dy:YAG as Function of Temperature.

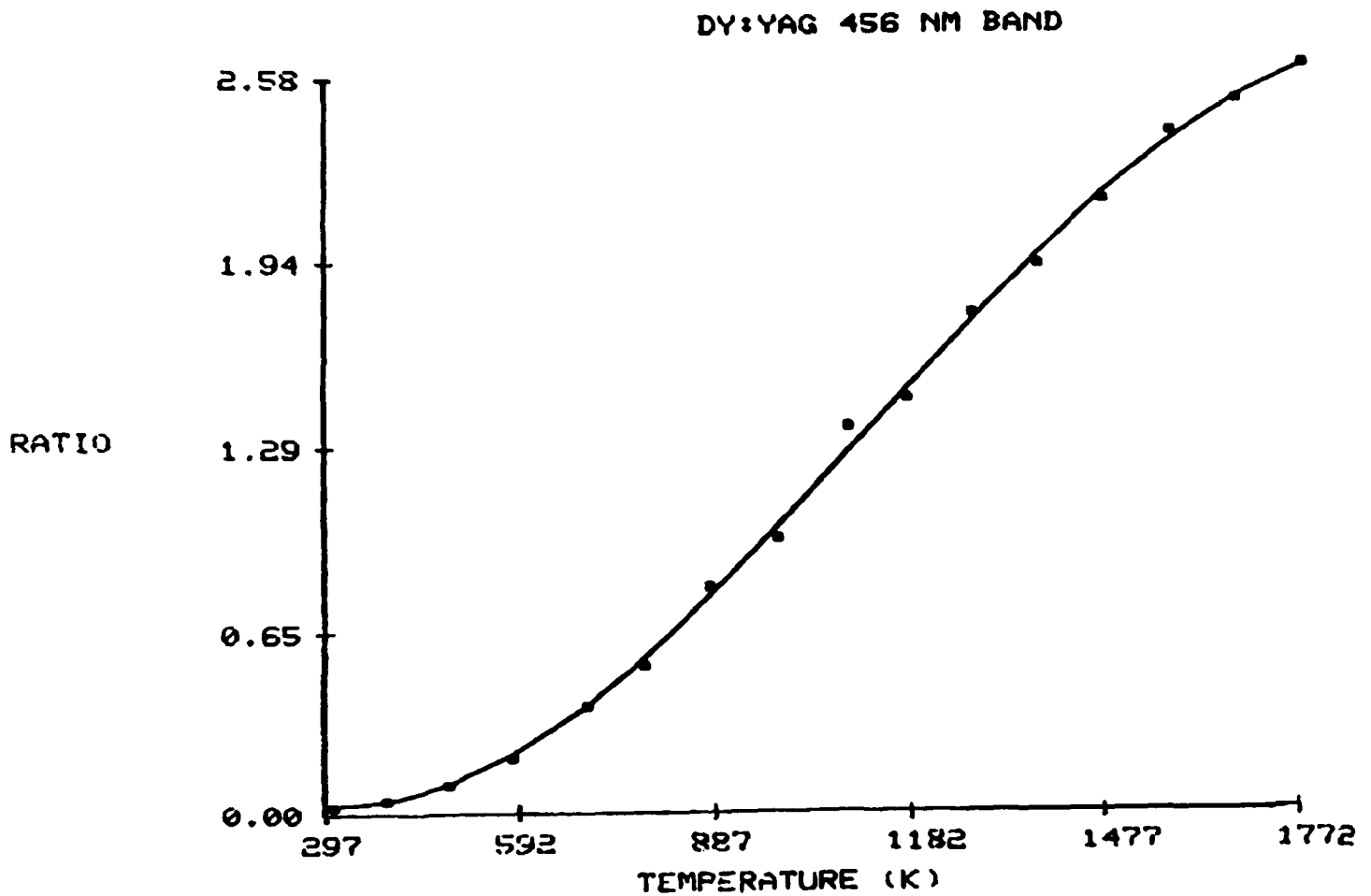

Figure 6. Variation of Relative Intensity of 456-nm G-Level Stark Component to 496-nm F-Level of Dy:YAG as Function of Temperature.

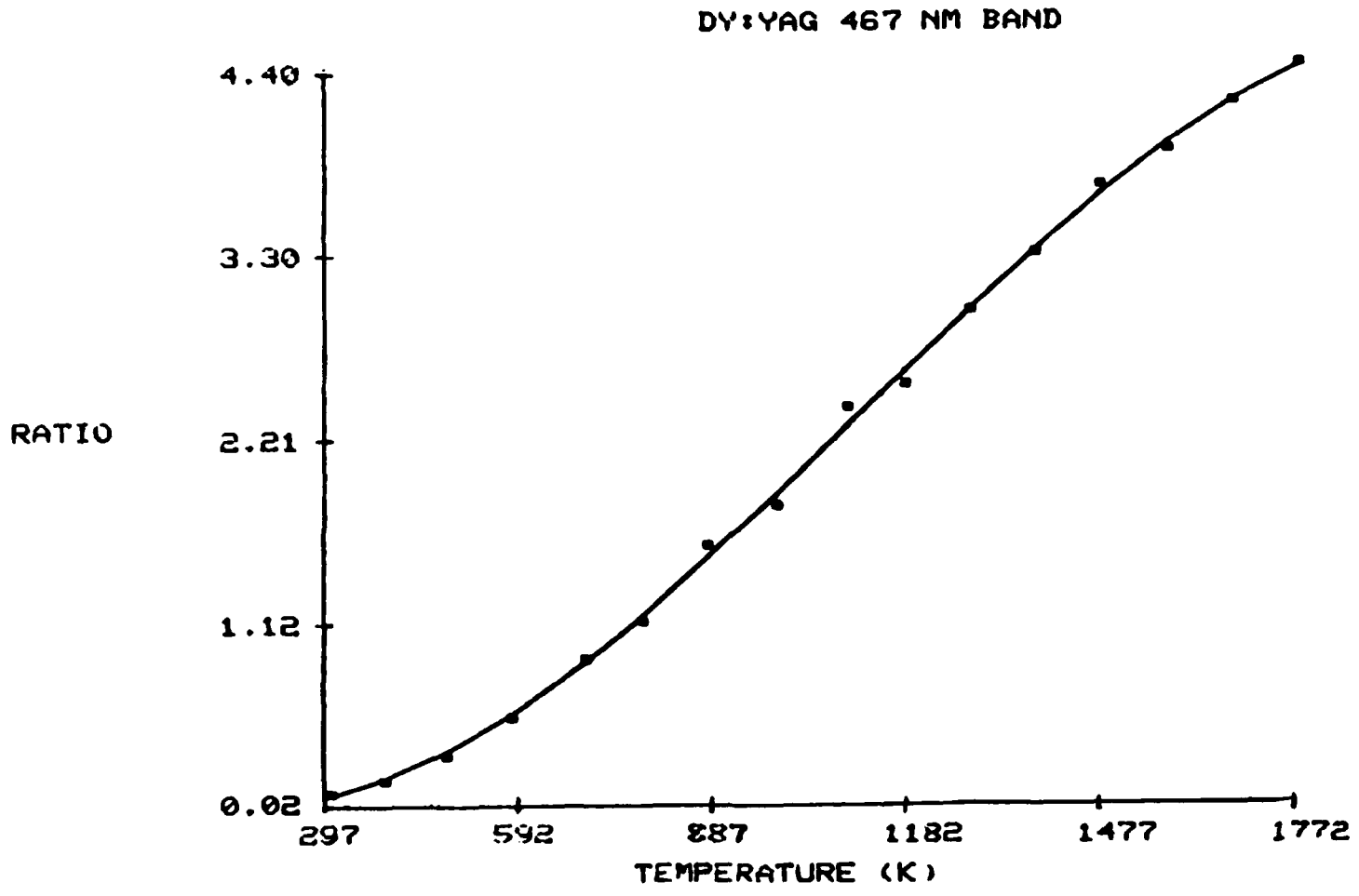

Figure 7. Variation of Relative Intensity of 467-nm G-Level Stark Component to 496-nm F-Level of Dy:YAG as Function of Temperature.

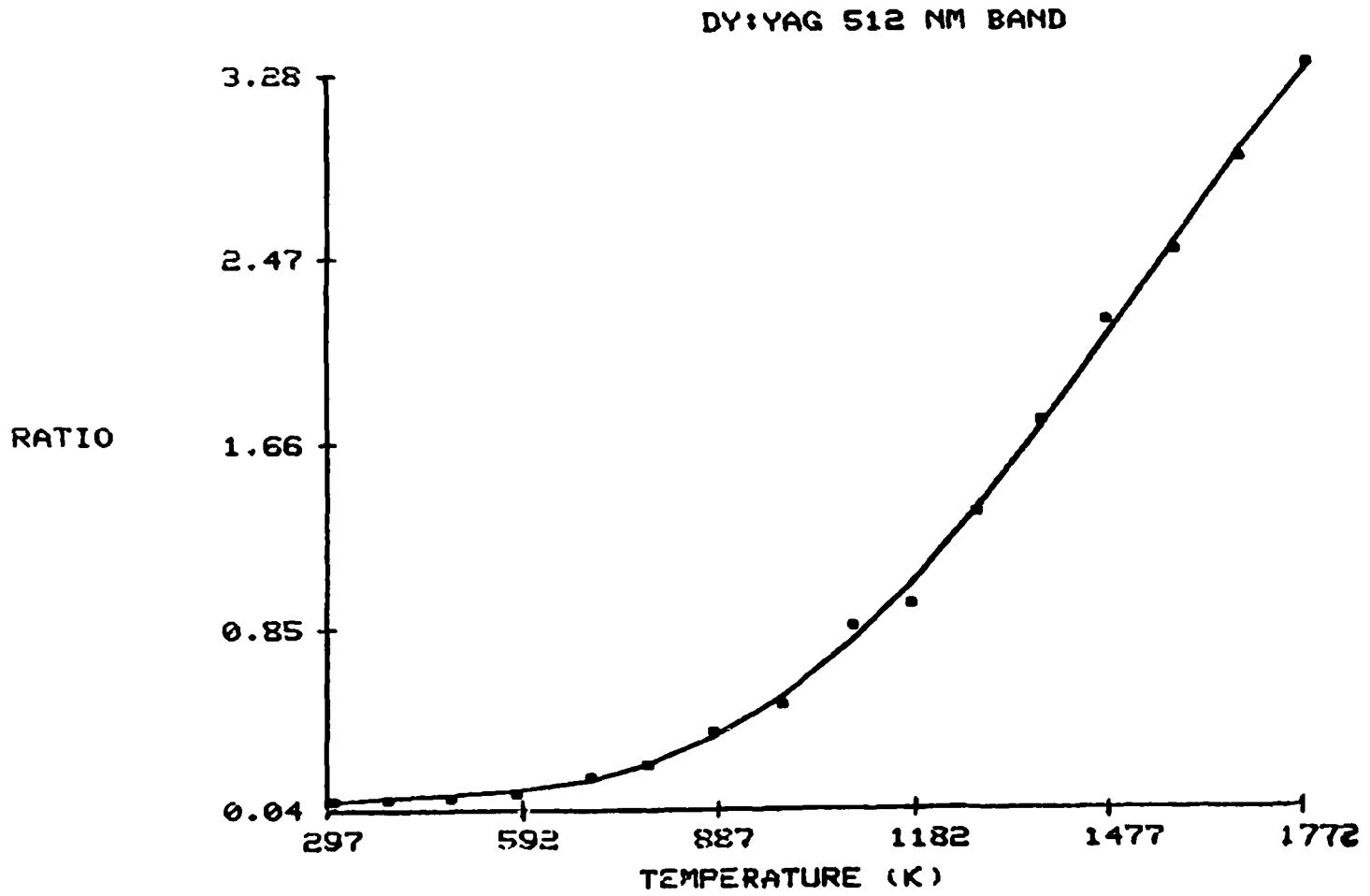

Figure 8. Variation of Relative Intensity of 512-nm Line to 496-nm F-Level of Dy:YAG as Function of Temperature.

3.2 Temporal Response of Particles

To function as a surface-temperature indicator, the crystals must be sufficiently small to permit accurate tracking of the temperature fluctuations which may occur on the surface being studied. To gain insight into just how small the particle must be, the thermal wavelength can be examined. The thermal wavelength is defined as the depth to which a thermal wave of frequency f can travel through a material and sustain only a 1/e attenuation of its amplitude. Mathematically the thermal wavelength is given by

$$\lambda_T = \sqrt{\frac{k_p}{\rho_p C_p \pi f}} \qquad (2)$$

where ρ_p is the particle density, k_p the thermal conductivity, and C_p the particle specific heat. Table I gives the thermal wavelengths for various frequencies for a YAG crystal.

Table I

THERMAL WAVELENGTH FOR YAG AS FUNCTION OF VARIOUS THERMAL-WAVE FREQUENCIES

Frequency (Hz)	λ_T (μm)
10	254
100	81
1,000	25
10,000	8

If the temperature field is uniform throughout the crystal, then the temporal response of the crystal can be described by

$$\tau \frac{dT_c}{dt} = T - T_c \tag{3}$$

where τ is the crystal time constant, T_c is the crystal temperature, and T is the surrounding temperature. This is the commonly used equation for a thermocouple in which the time constant is given by

$$\tau = \frac{\rho_c C_c d_c^{1.5}}{1.92K\sqrt{\frac{\rho_s u_s}{\mu_s}}} \tag{4}$$

where ρ_c = density of the YAG crystal
C_c = specific heat of the crystal
K = thermal conductivity
d_c - diameter of the crystal

The transfer function which describes the crystal response to a given thermal frequency is given by

$$y(f) = \frac{1}{1 + j2\pi f\tau} \tag{5}$$

This transfer function is characterized by a flat response up to the rolloff frequency, followed by a 6-dB/octave drop. The cutoff frequency at which the response begins to drop off (3-dB drop) is defined as follows:

$$f_c = \frac{1}{2\pi\tau} \tag{6}$$

The cutoff frequency as a function of crystal size is tabulated in Table II. The table indicates that a particle 5 μ or less in size could easily track the thermal variations expected on a reacting surface.

Table II

ROLLOFF FREQUENCY AND TIME CONSTANT OF YAG CRYSTALS
AS FUNCTION OF PARTICLE SIZE

d (μm)	τ(μs)	F_c (Hz)
100	1770	90
50	626	255
10	56	2,850
5	20	8,065
1	2	90,165

3.3 Thermographic Imaging

One of the major advantages of employing LIF with thermographic phosphors is the possibility of using one- and two-dimensional detectors to record line and entire-surface temperature distributions. By simultaneous monitoring of the F- and G-levels of Dy:YAG, the surface temperature at a point along a line or over the entire surface can be determined with appropriate detectors.

The experimental arrangement used for surface thermographic imaging is shown in Fig. 9. The main component of the system is a 1024-element intensified diode array (Tracor Northern TN1710). The fluorescence from the surface is excited by the 355-nm tripled output of a Quanta-Ray Nd:YAG laser. The output of the laser is an $\sim$ 8-ns pulse which pumps the Dy:YAG into a highly excited electronic state. Through radiative and nonradiative decay processes, the F- and G-fluorescence levels become populated. The lifetime of the levels decreases with temperature elevation.

The intensified detector is gated with a 10-μs pulse which is an aid in discriminating against unwanted background radiation from the surface. This feature is very important at elevated temperatures where the

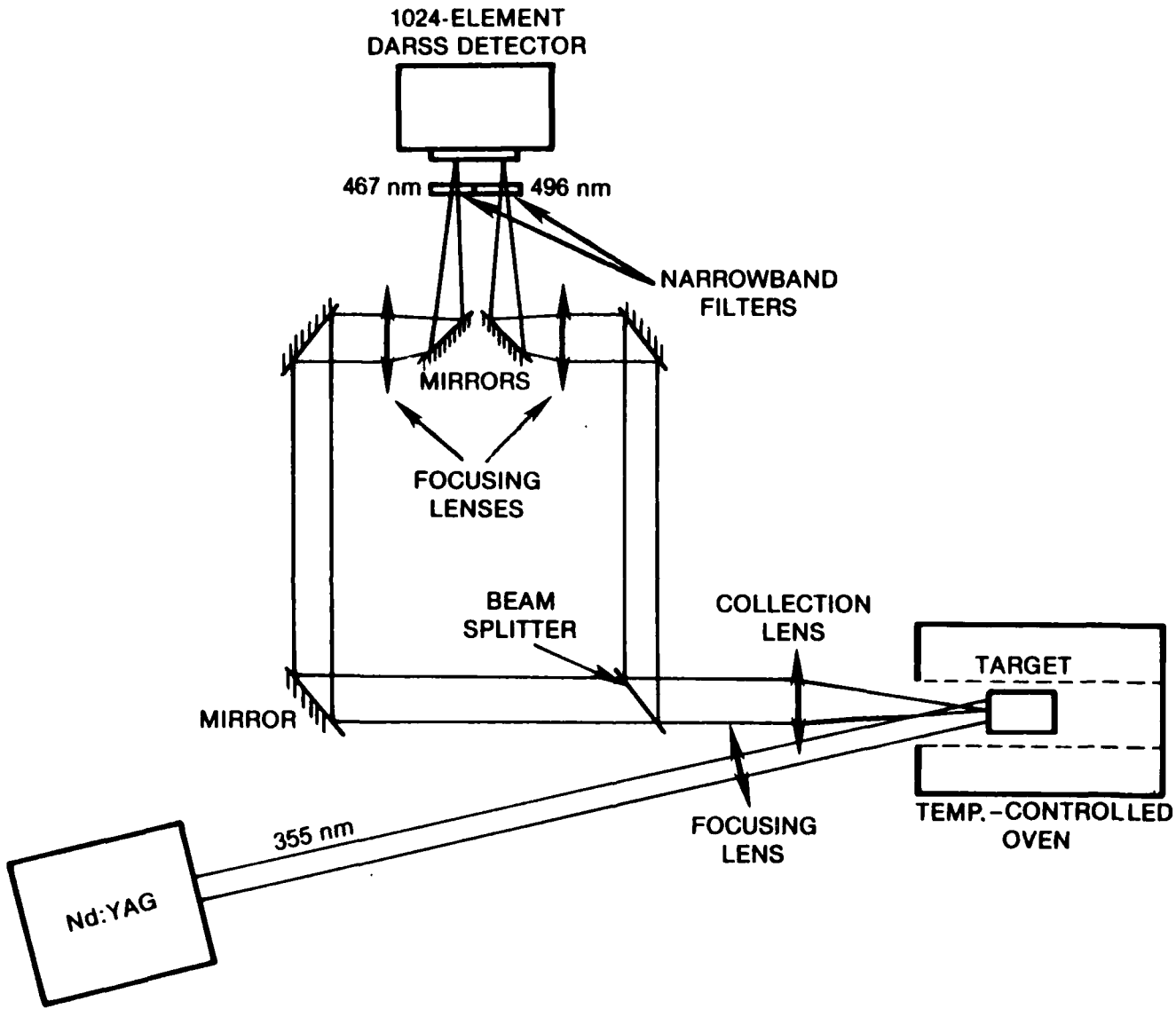

Figure 9. Experimental Arrangement for Surface Thermographic Imaging Utilizing Pt-Rh Thermocouple-Controlled Oven for Calibration.

natural blackbody emission from the surface and surroundings can be particularly high.

The fluorescence from the surface is collimated by an F-6 lens, split into two equal paths, and directed through 496- and 467-nm filters for the F- and G-level fluorescence, respectively; the two paths are imaged side by side on the DARSS detector. Great care was taken to prevent path differences between the two legs and matched imaging lenses were used, which helped to ensure that the images at the two wavelengths would be spatially identical.

The video signal from the DARSS detector is digitized, stored in a temporary memory, and subsequently sent to a ModComp minicomputer. The data are stored on disk for analysis at a later date. The limited rate of data transfer is determined by the 10-Hz operation of the Nd:YAG laser.

Image analysis consists of ratioing the F- and G-fluorescence signals and converting the resulting signal to a temperature with the aid of calibration curves established using a platinum-coiled oven. The surface temperature can then be examined as a function of time and/or space.

Calibration of the system was performed with the platinum-coiled oven which is capable of temperatures in excess of 1723 K. The calibration target was ceramic formed around a Pt-Rh thermocouple. The face of the ceramic was coated with a layer of Dy:YAG particles, $\leq$ 20 μm in diameter. The overall oven temperature was monitored with another Pt-Rh thermocouple mounted $\sim$ 1.25 cm above the target. As each preset temperature was achieved, the oven was held at that temperature for 30 minutes to ensure overall temperature stability. The first setting was at room temperature ($\sim$ 293 K) and the second at 323 K. Subsequent temperature settings were in 50-K increments to a maximum of 1673 K.

The results of one of these runs are shown in Fig. 10. The 29 plots on the left are intensity plots of the 496-nm line, and those on the right are for the 467-nm line. A plot of the ratio of 467- to 496-nm intensity is shown in Fig. 11.

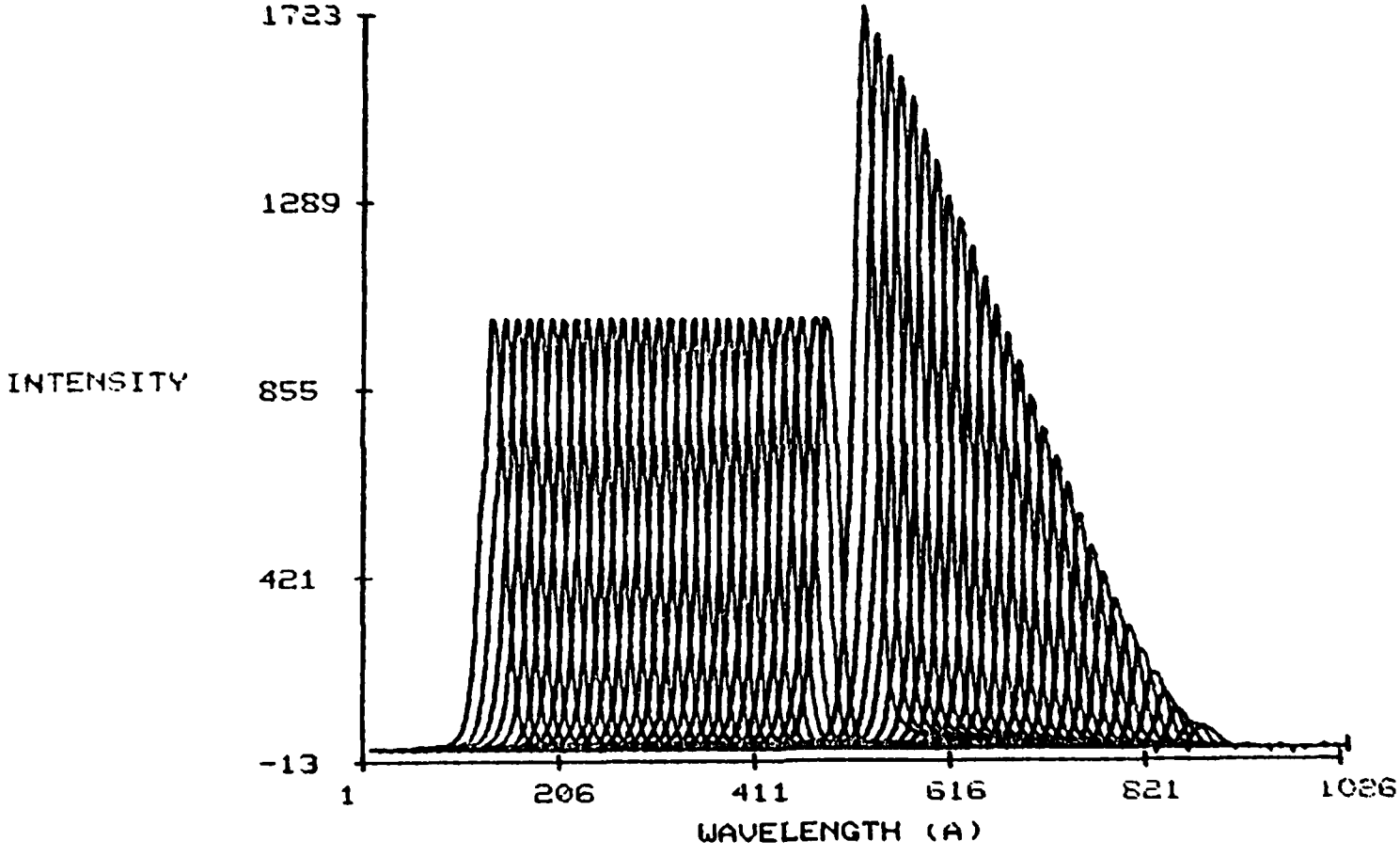

Figure 10. F- and G-Level Fluorescence as Function of Temperature from 300 to 1673 K in 50-K Increments.

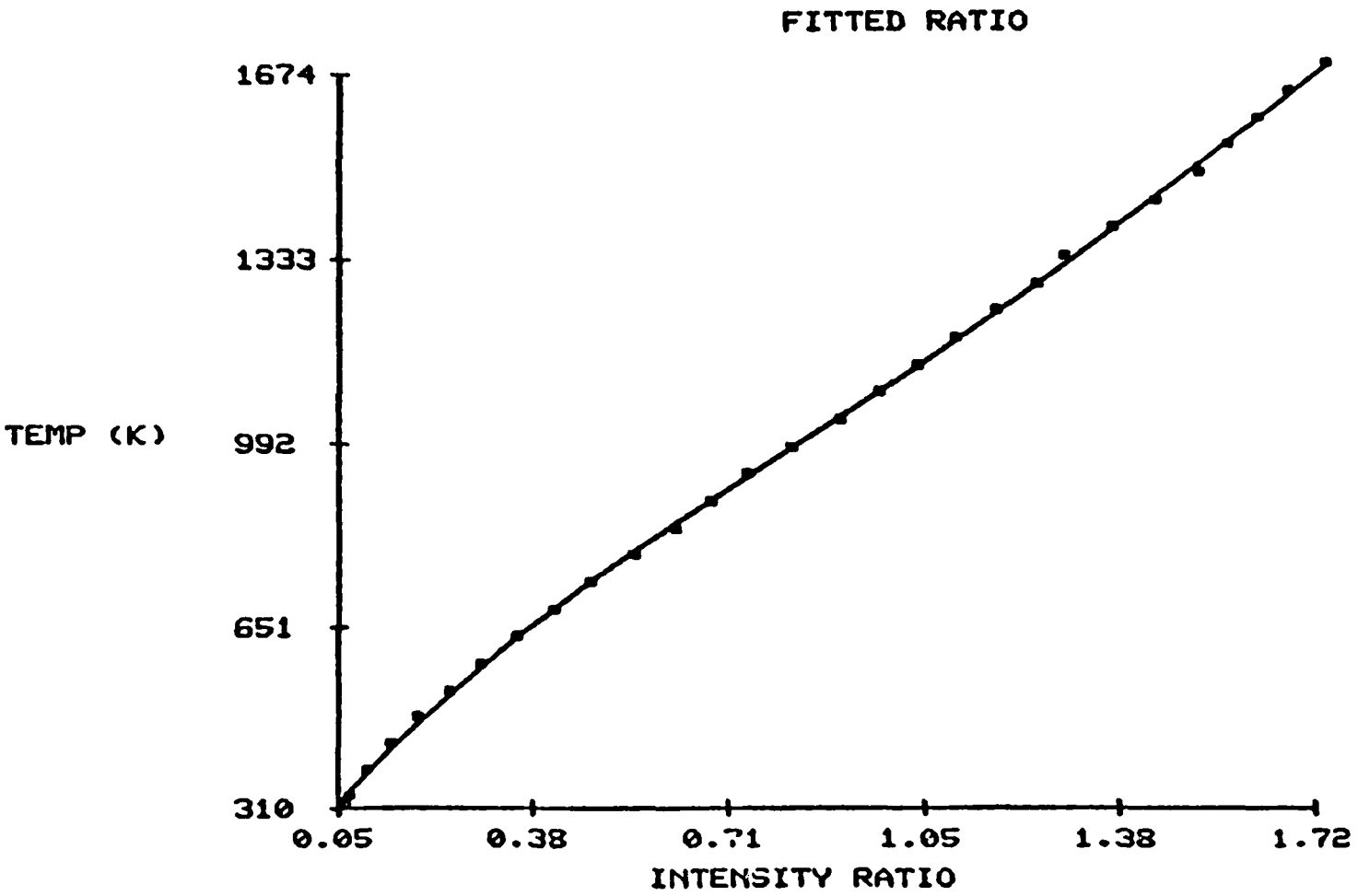

Figure 11. Ratio of Intensity of G-Level Stark Component (467 nm) to F-Level (496 nm) Dy:YAG as Function of Temperature.

The LIF signal is extremely reproducible as a function of temperature and, thus, the accuracy of the LIF technique is directly linked to the accuracy of the thermocouple which is used for calibration. This is in the range 1 - 10 K, depending upon the absolute temperature. The precision of the measurement is affected by a number of factors, including photon statistics, detector noise, and background signal levels. With the large signal levels from the Dy:YAG crystals, the major limit to precision is the detector noise which is $\sim$ 3%. Thus, in a single-shot mode of operation, a $\pm$ 9 - $\pm$ 50 K uncertainty is observed in the 300 - 1500 K temperature range.

Two target materials were used for these studies. The first was constructed of ceramic with Dy:YAG crystals bonded into the face (Fig. 12). This target was utilized for all high-temperature tests to prevent erosion of the surface. The second material was a pressure-thermal-setting plastic produced by Buehler, Ltd. This target is made by mixing 7 g of the plastic powder with 1 g of 20-μm Dy:YAG crystals. This mixture is then pressed to $\sim$ 4000 psi and heated for 20 minutes at 523 K. This produces a cylindrical plastic target 2.54 cm in diameter and 1.25 mm thick (see Fig. 13).

3.4 Nonreacting-Surface Thermography (Embedded Wire, Torch, and CO_2-Laser-Heating Studies)

The initial temperature measurements on a nonreacting surface were made using the experimental arrangement shown in Fig. 14(a). The surface consisted of small (< 50 μ) Dy:YAG crystals implanted in a ceramic material in which a small Nichrome wire had been embedded. An electrical current was allowed to flow through the wire to act as a local heat source, and the fluorescence from the 467-nm G-Stark component was monitored by a linear multichannel detector along a line perpendicular to the wire filament. The fluorescence was recorded in a single 10-ns pulse and stored by the ModComp computer to obtain a time history of the temperature changes at the surface under heat-up and cool-down conditions [14(b-c)]. Under heat-up conditions [14(b)], the initial rise in temperature is centered at the embedded wire, with a gradual transfer of

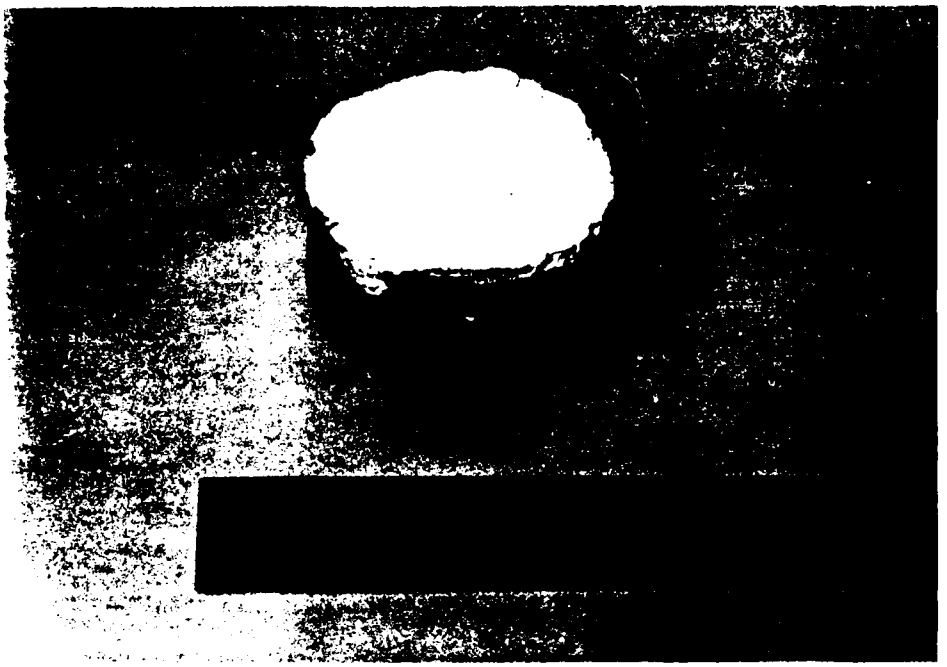

Figure 12. Ceramic Target Material with Dy:YAG Crystals Bonded into Face.

Figure 13. Cylindrical Plastic Target Doped with Dy:YAG Crystals.

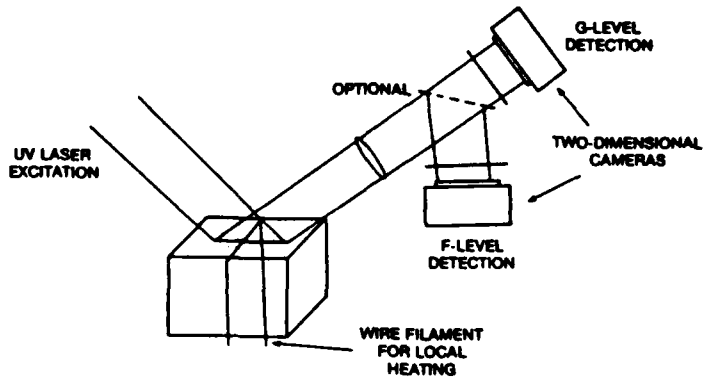

(a)

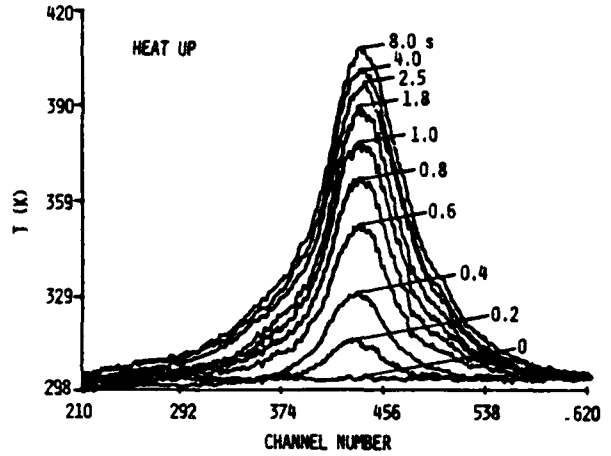

(b)

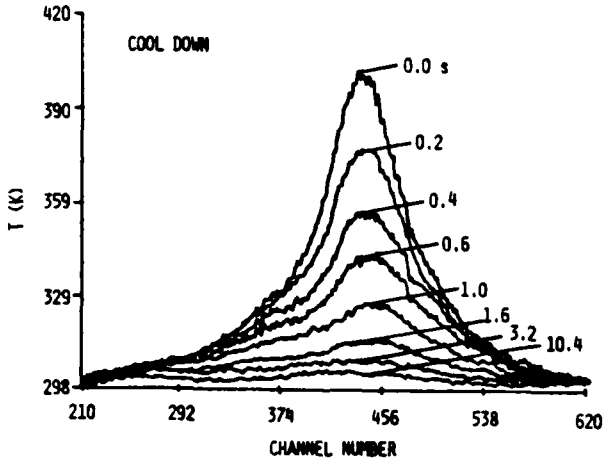

(c)

Figure 14. (a) Experimental Setup for Surface-Thermometry Studies, (b and c) Temporal Variation of Surface Temperature of Ceramic Material under Heat-up (b) and Cool-Down (c) Conditions.

heat to the surrounding surface. After 22 seconds, the maximum temperature rise is observed in the area surrounding the embedded wire (400 K). The heat buildup after this point is slower, asymptotically approaching 420 K. The cooling of the surface after interruption of electrical current to the wire filament is shown in Fig. 14(c). The temperature decline is steep in the peak-temperature area but slows as the central temperature approaches that of the surrounding heated area.

Because a nonreacting surface was examined in this case, only the G-fluorescence level of Dy:YAG was monitored. However, on reacting surfaces or in situations where an absolute measurement is difficult, both the G- and F-fluorescence signals must be monitored. The experimental setup in Fig. 9 was used for this purpose, with the calibration oven being replaced by the embedded ceramic. The experiment which involved heating the surface by means of the embedded wire was then repeated with this arrangement, all conditions being nearly the same except that a larger electrical current was allowed to flow through the wire which resulted in a higher surface temperature. In this second case the temporal history of the surface temperature was tracked over two heating and cooling cycles covering a 50-second period or 500 laser shots. The fluorescence images observed by the DARSS detector are plotted in Fig. 15. The ratio of the images is converted to a temperature and plotted in Fig. 16. The current is turned on $\sim$ 3 seconds after data acquisition is initiated, which is indicated by the fast rise in surface temperature. At approximately the 8-second point, a maximum temperature of 600 K is reached. The current is then extinguished and the surface cools with an almost exponential decay in surface temperature. After $\sim$ 38 seconds the electrical current is turned on again, and a second heat cycle is observed. During this cycle the maximum temperature of 644 K was obtained. By examining only a single channel (spatial point on the surface), a detailed temporal history can be recorded, which represents what would be recorded by a thermocouple or point-measurement technique. The heat-up and cool-down cycles are clearly displayed in Fig. 17. The spatial location corresponds to the peak of the temperature profile (near the embedded wire).

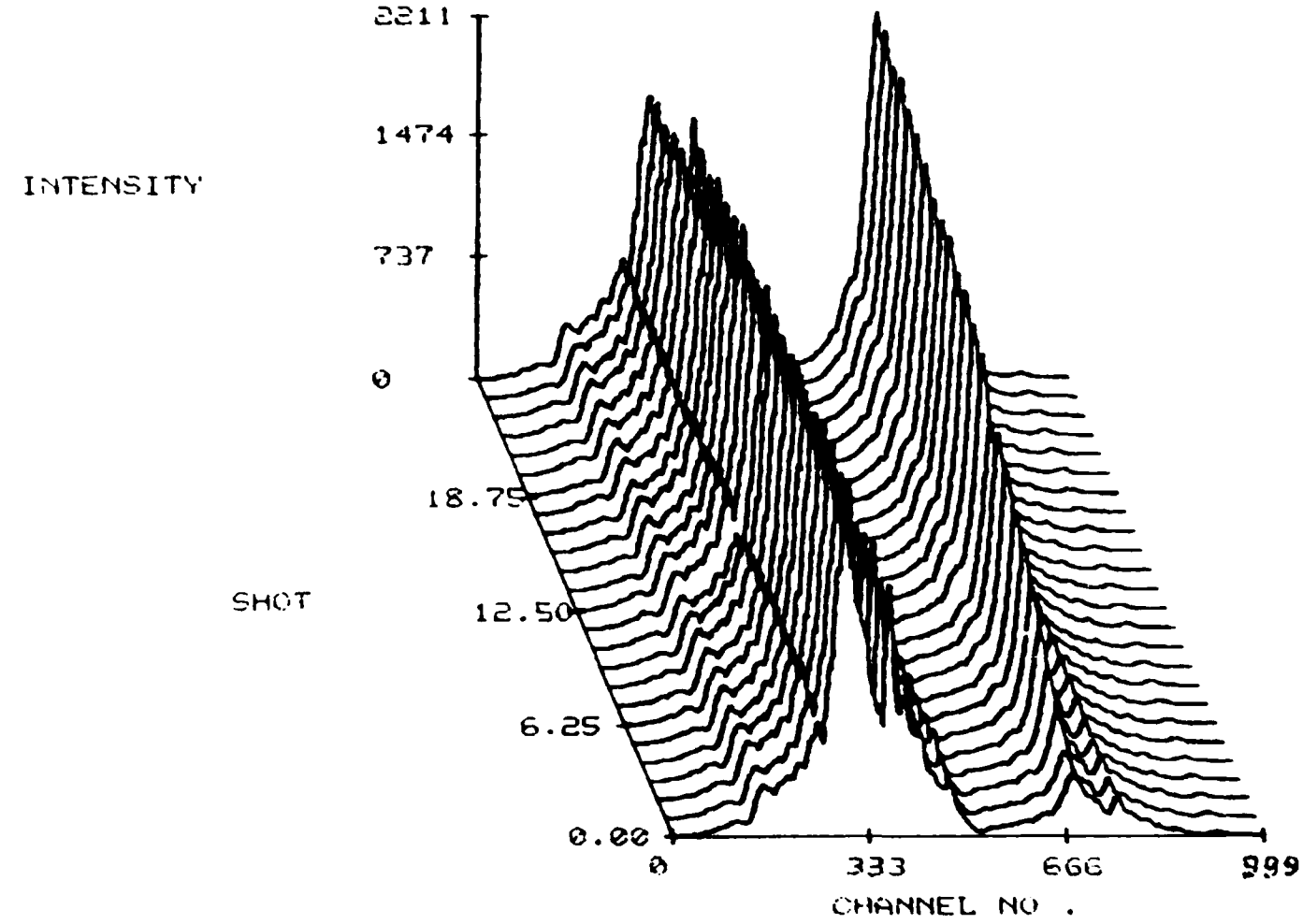

Figure 15. Plot of Fluorescence Intensity of Ceramic Target with Heating Wire Imbedded Showing 496- and 467-nm Lines as Observed by DARSS Detector.

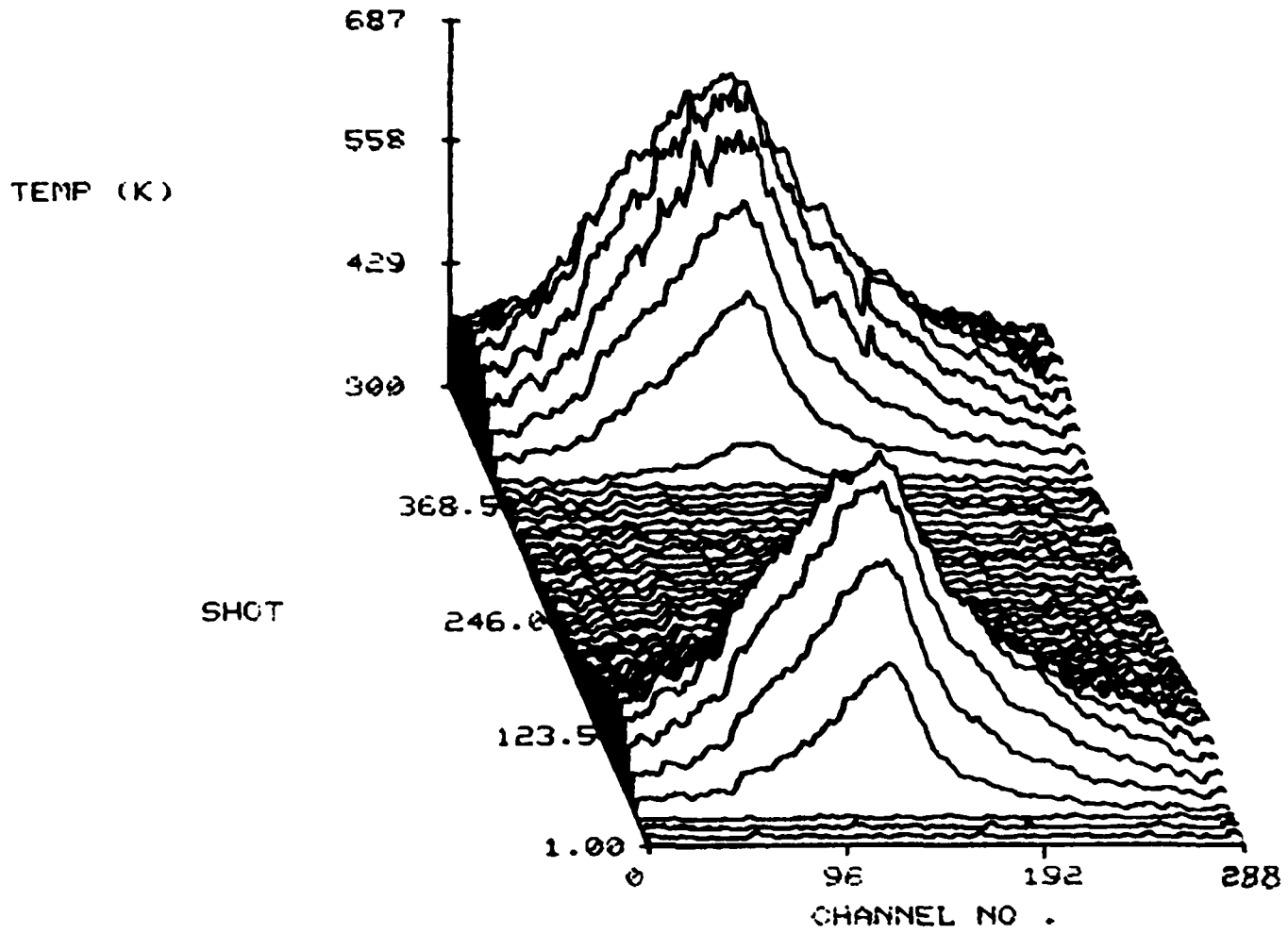

Figure 16. Temperature Plot Resulting from Fig. 15 with Two Heating Cycles Viewed Spatially over ~ 1 cm.

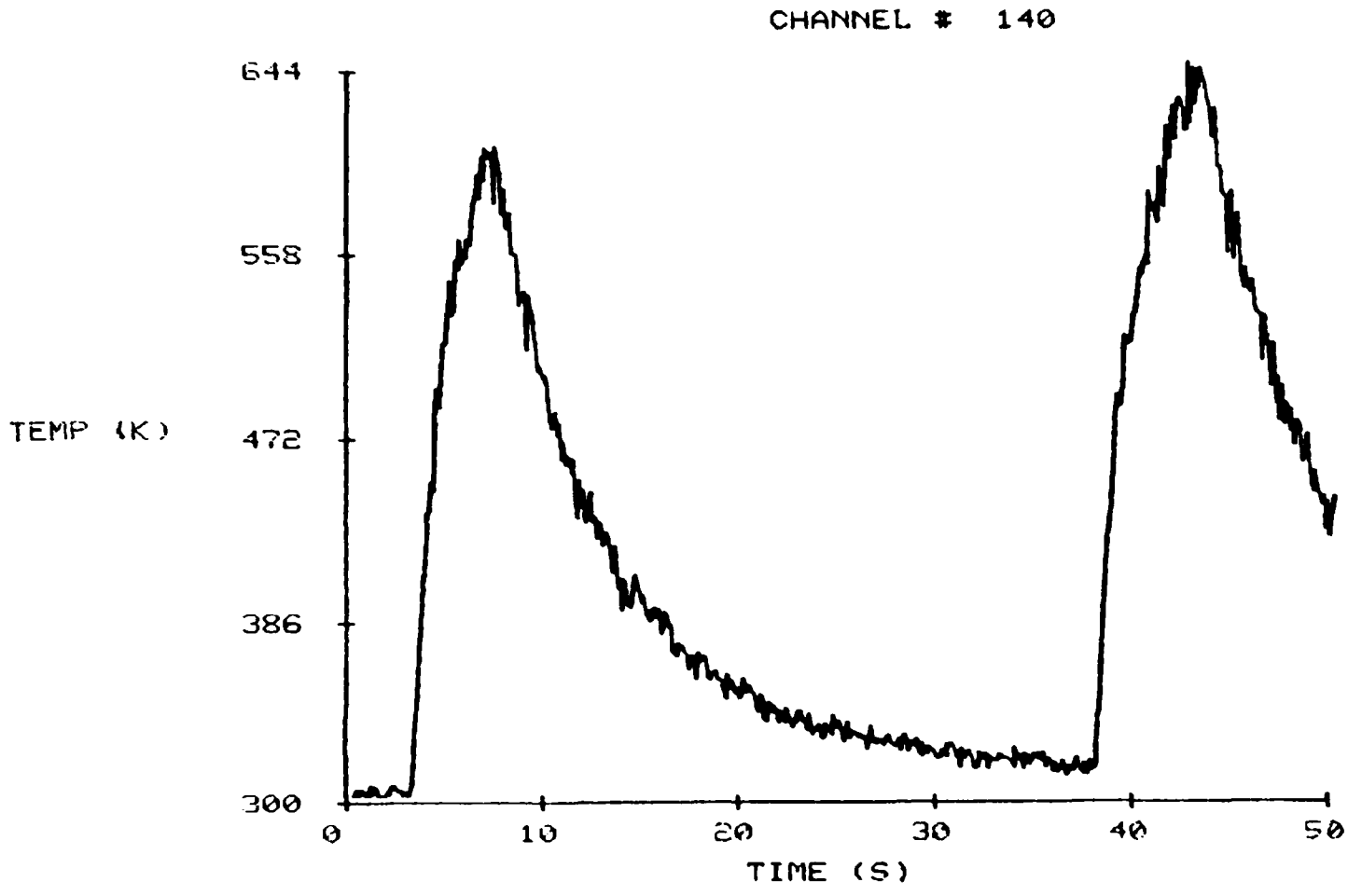

Figure 17. Plot of Heat-Up and Cool-Down Cycles of Ceramic Target With Heating Wire Imbedded.

To illustrate the effects of a near-uniform heat source, a propane-air premixed torch was used to heat the ceramic surface. The area which was imaged is ∿ 1 cm in length; the fluorescence signals are shown in Fig. 18. The ratio of these signals yields the temperatures shown in Figs. 19 and 20. The nearly constant temperature profile is consistent with the heat source. The temporal history is displayed in Fig. 21. Two heat-up and cool-down cycles were examined. Notice that in the initial heat-up cycle, an interruption is observed ∿ 6 seconds after initiation of data acquisition. This interruption corresponds to a movement of the torch which was hand-held.

To illustrate the effects of rapidly heating the surface, a 100-W CO_2 laser was used to heat the ceramic surface. The experimental arrangement for this study is shown in Fig. 22. The CO_2 laser beam was incident on the surface at an angle of ∿ 45 deg. This resulted in a skewed temperature distribution, as will be demonstrated. In these experiments ∿ 14 W of CO_2 power was distributed over a 2-mm spot size. Three heat-up and cool-down cycles were examined with this setup. The experimental fluorescence data are shown in Fig. 23. The temperature profile of the first-cycle heating is displayed in two-dimensional form in Fig. 24. This figure demonstrates the large skewed temperature distribution. The initial temperature rise is symmetric and then becomes skewed with time because of the angle of the incident beam. This is displayed in the three-dimensional plot in Fig. 25. The heat rise on the surface is quite rapid, going from 300 to 792 K in ∿ 1 second. The three-dimensional plot of all three heat-up and cool-down cycles is shown in Fig. 26, with the temporal history being shown in Fig. 27. This clearly demonstrates the ability of the Dy:YAG crystals to track the rapid temperature changes which occur at the surface.

3.5 Reacting-Surface Thermography (CO_2-Laser-Heating Studies)

To demonstrate the thermometric technique on a surface similar to that of an energetic material, a thermal-setting plastic from Buehler, Ltd., was employed. The Dy:YAG crystals were mixed in a one-to-seven weight ratio with the plastic which was heated under pressure to form the test specimen. The plastic surface erodes as it is heated above 400 K and,

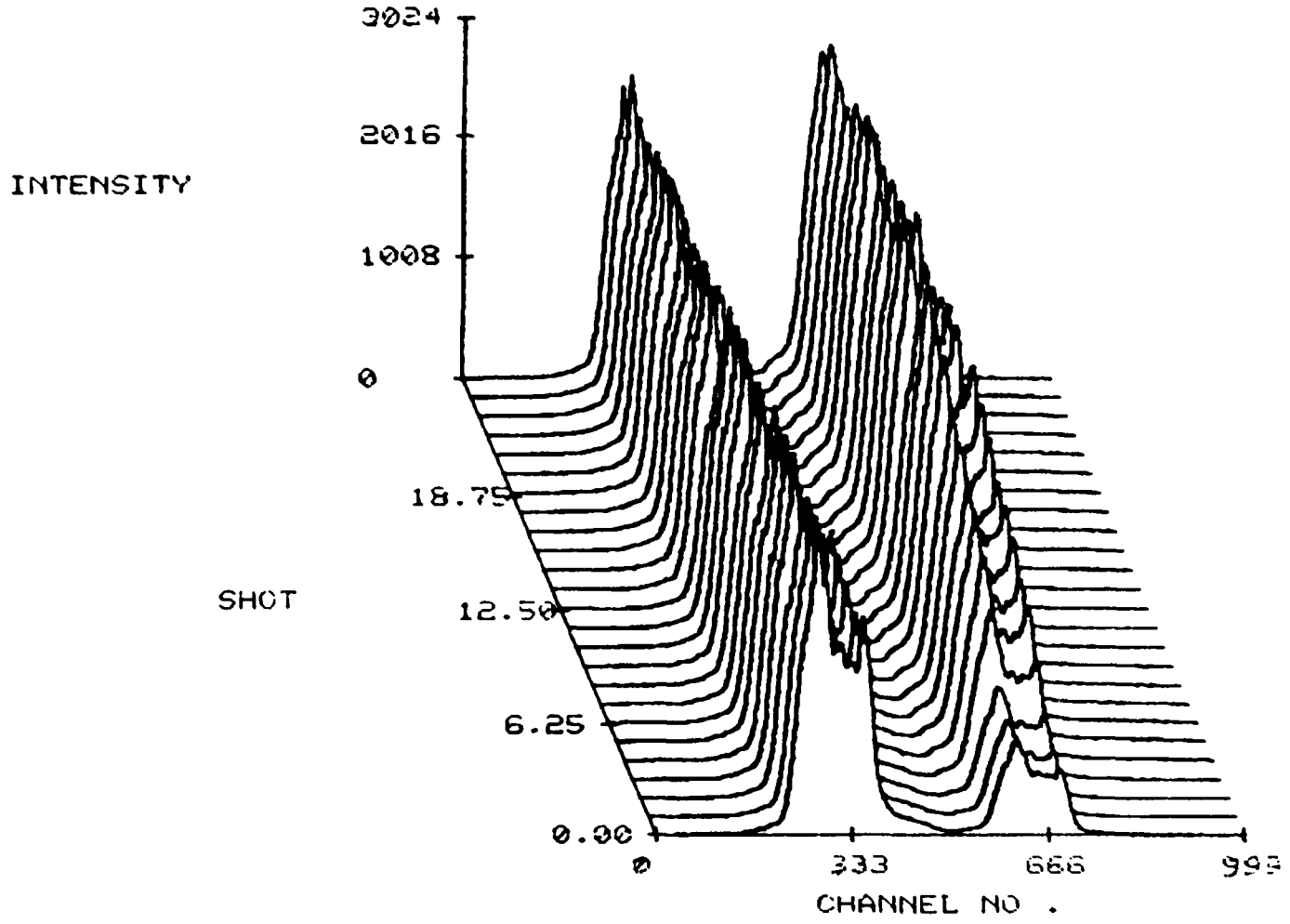

Figure 18. Plot of Fluorescence Intensity of Ceramic Target Heated with Propane-Air Premixed Torch Showing 496- and 467-nm Lines as Observed by DARSS Detector.

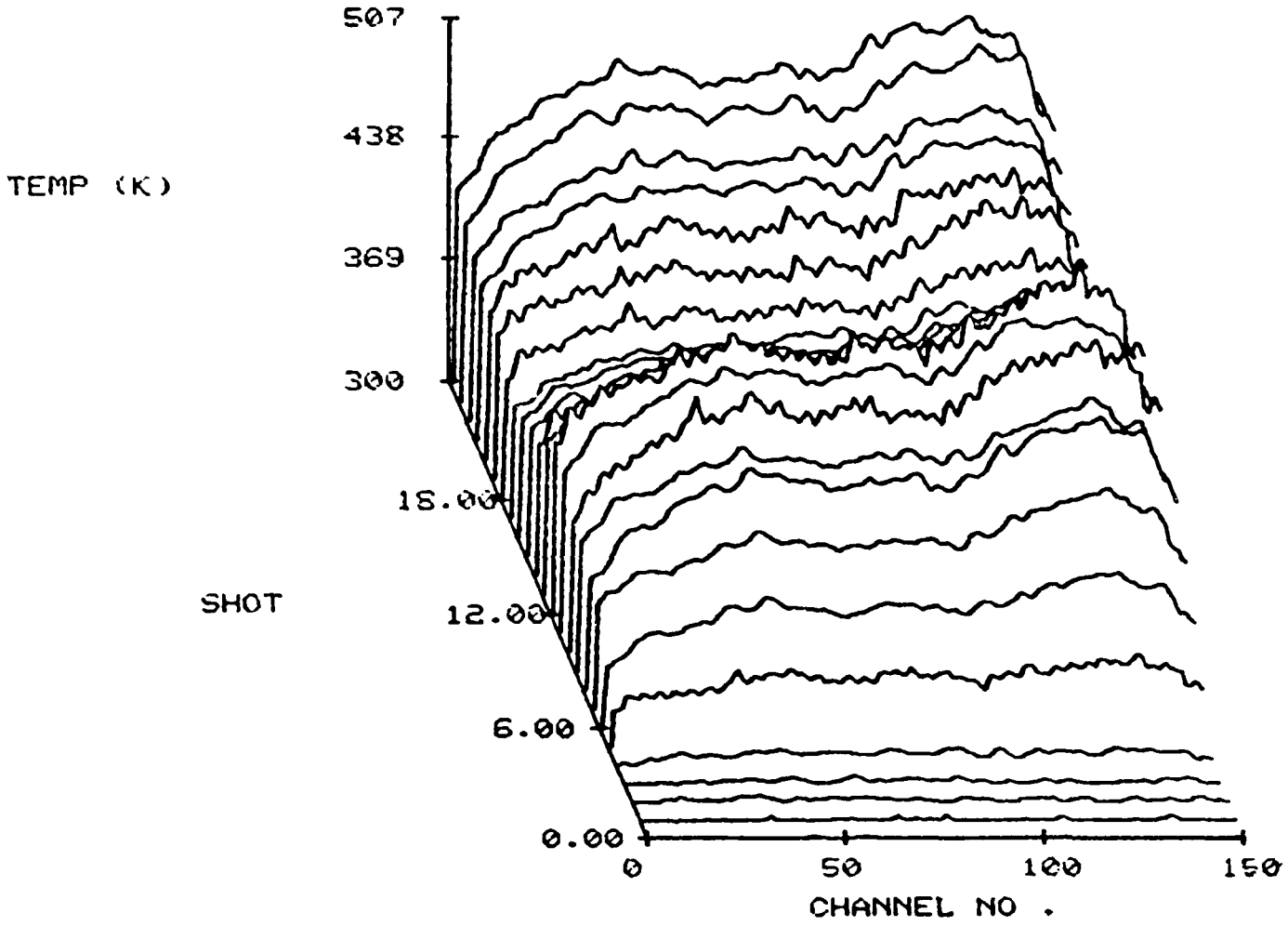

Figure 19. Temperature Plot Resulting from Fig. 18, First Heat-Up Cycle.

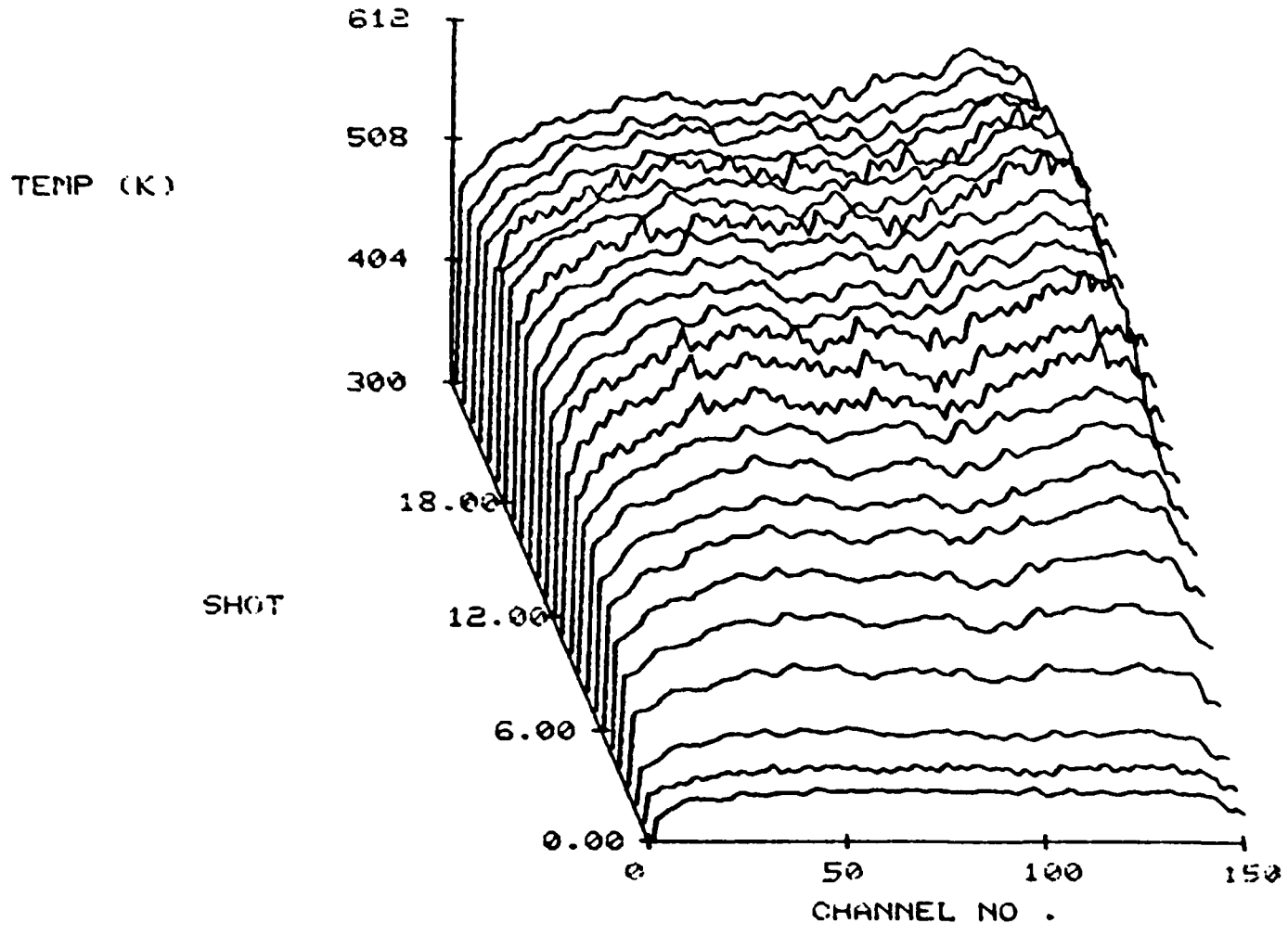

Figure 20. Temperature Plot Resulting from Fig. 18, Second Heat-Up Cycle.

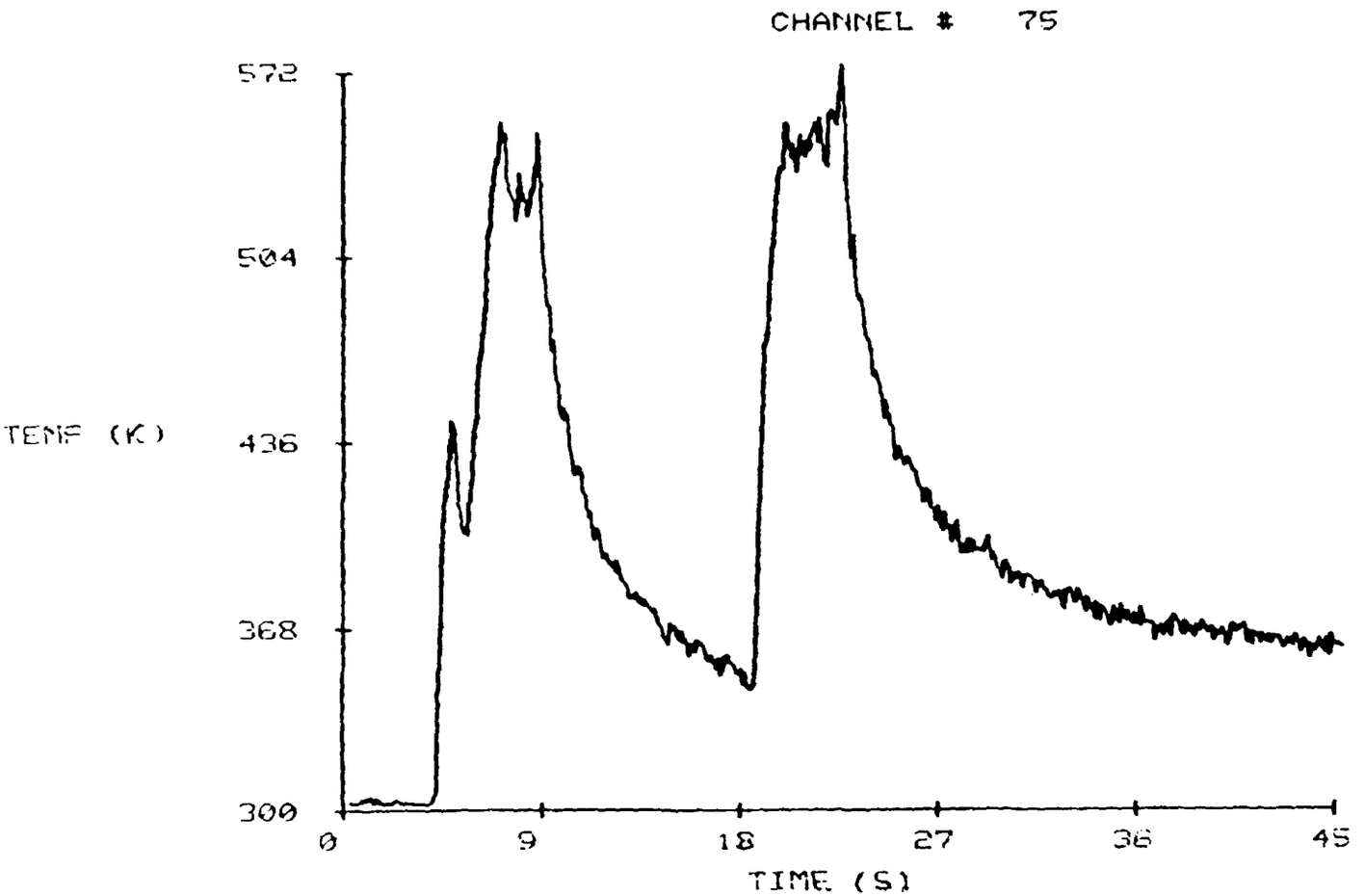

Figure 21. Heat-Up and Cool-Down Cycles of Ceramic Target Heated with Propane-Air Premixed Torch.

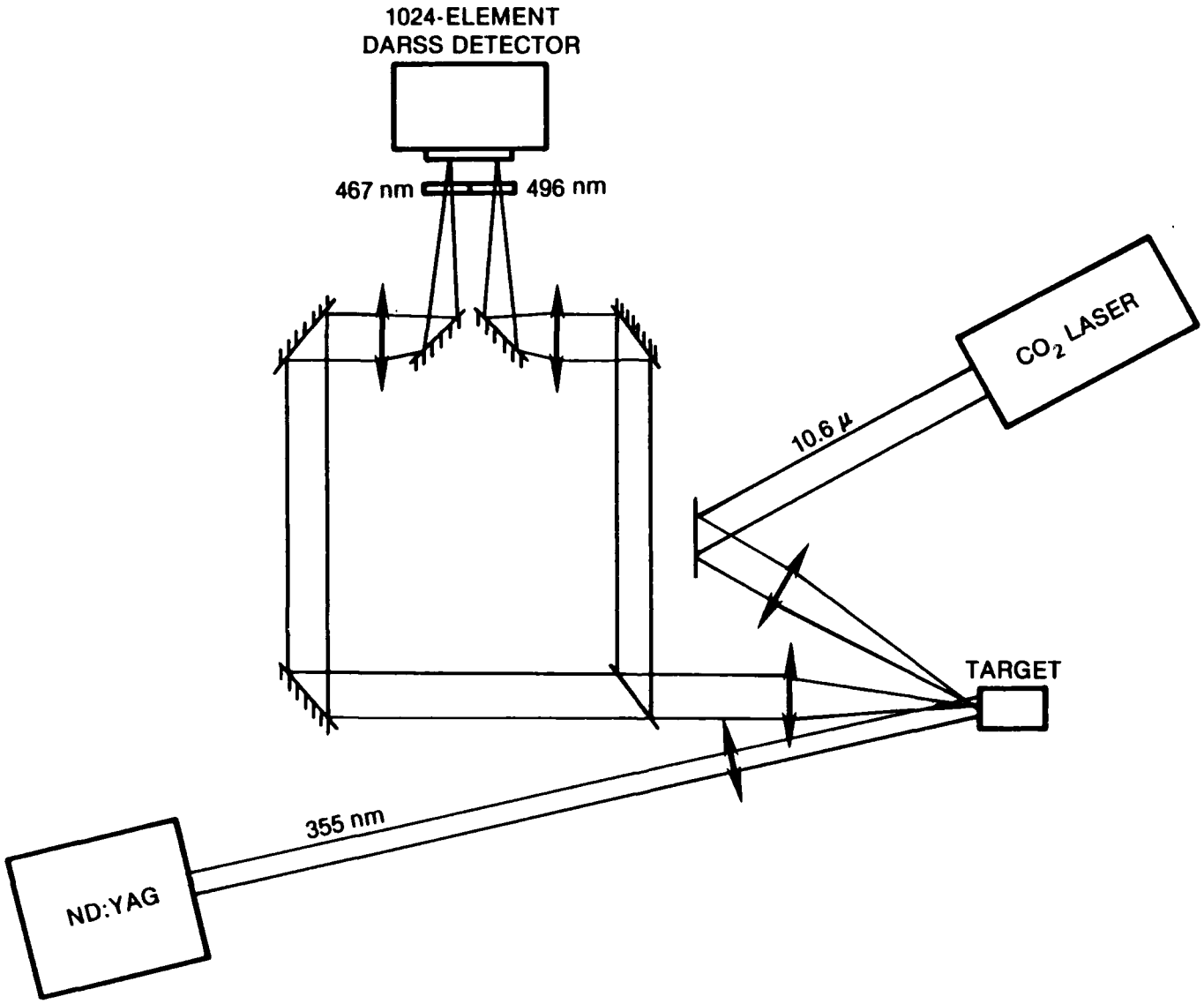

Figure 22. Experimental Setup for CO_2-Laser-Heated Surface-Thermometry Studies.

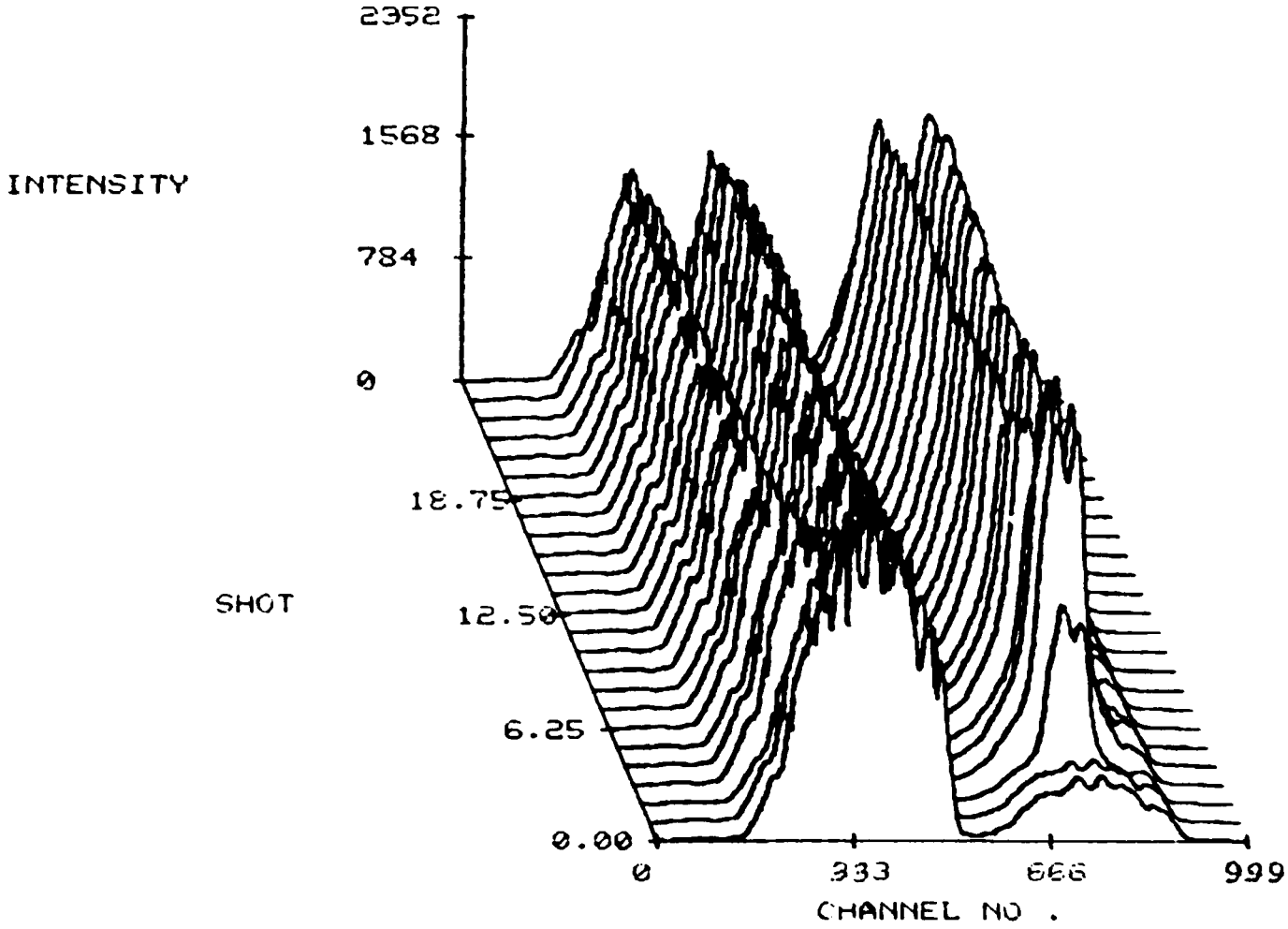

Figure 23. Plot of Fluorescence Intensity of Ceramic Target Heated with CO_2 Laser Focused to ∿ 2 mm Spot Showing 496- and 467-nm Lines as Observed by DARSS Detector.

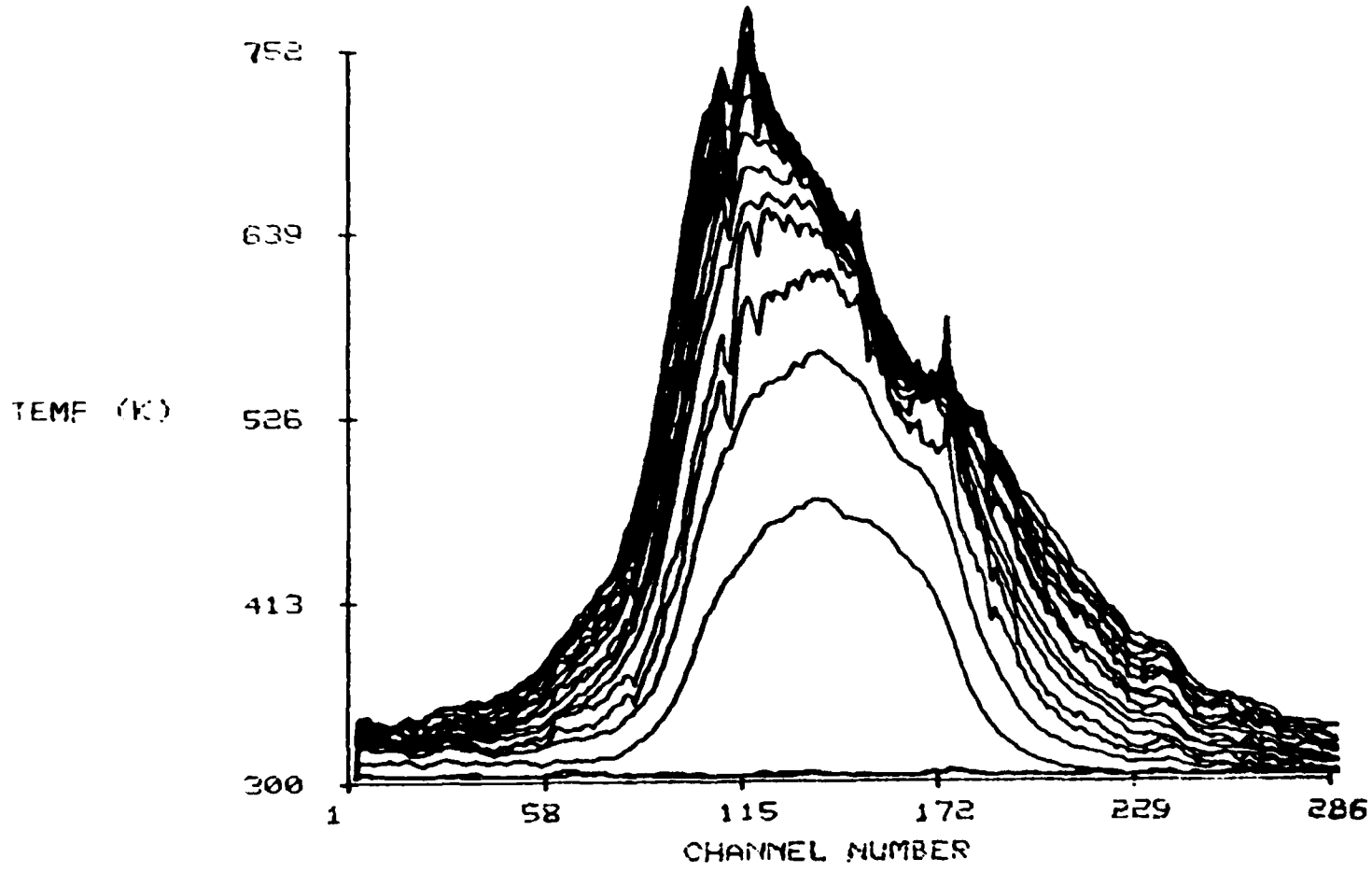

Figure 24. Temperature Profile of First Heating Cycle over ∿ 1 cm for Ceramic Target Heated with CO_2 Laser Focused to ∿ 2 cm Spot.

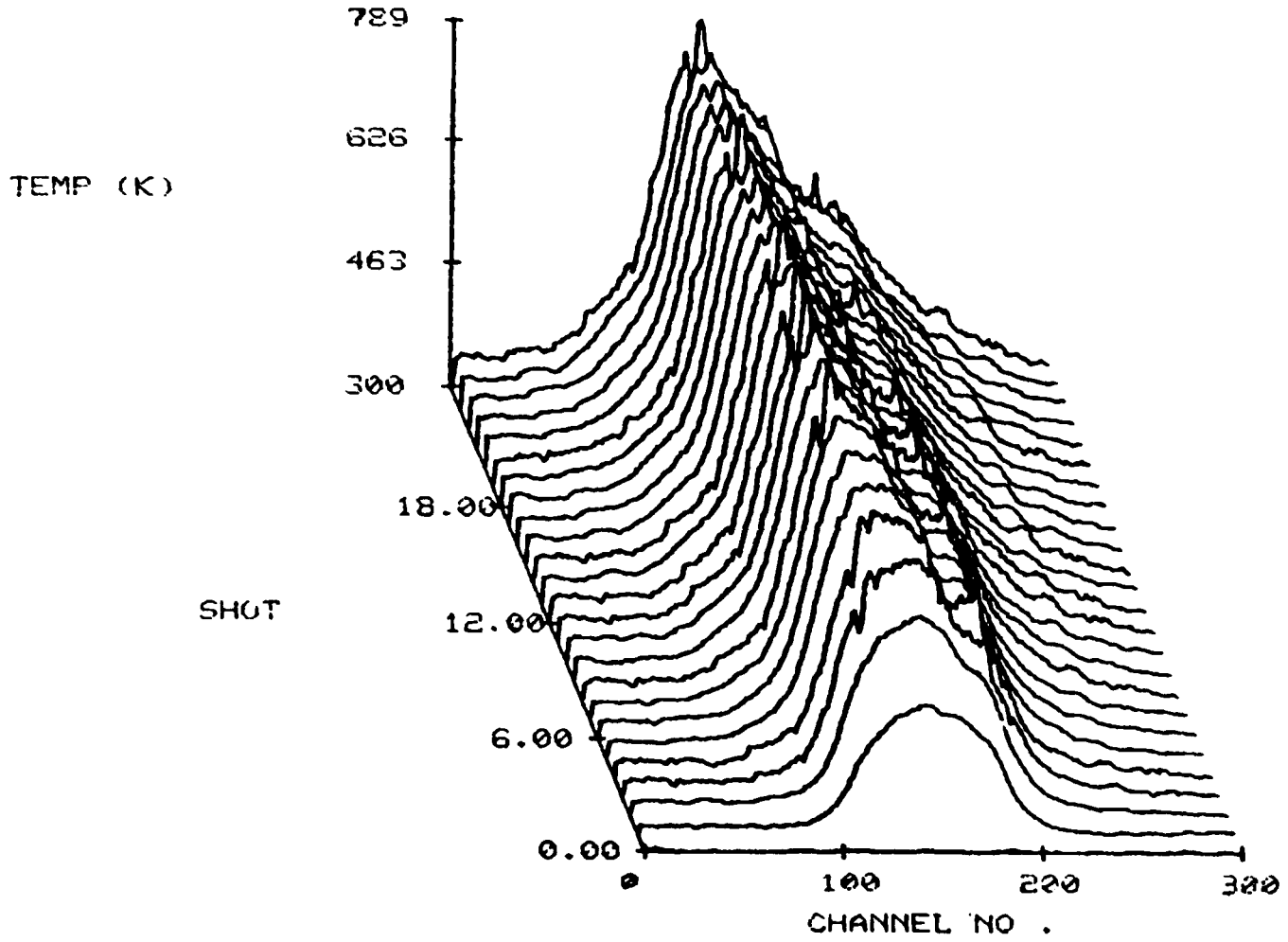

Figure 25. Three-Dimensional Plot of Temperature for Ceramic Target Heated with CO_2, First Heating Cycle.

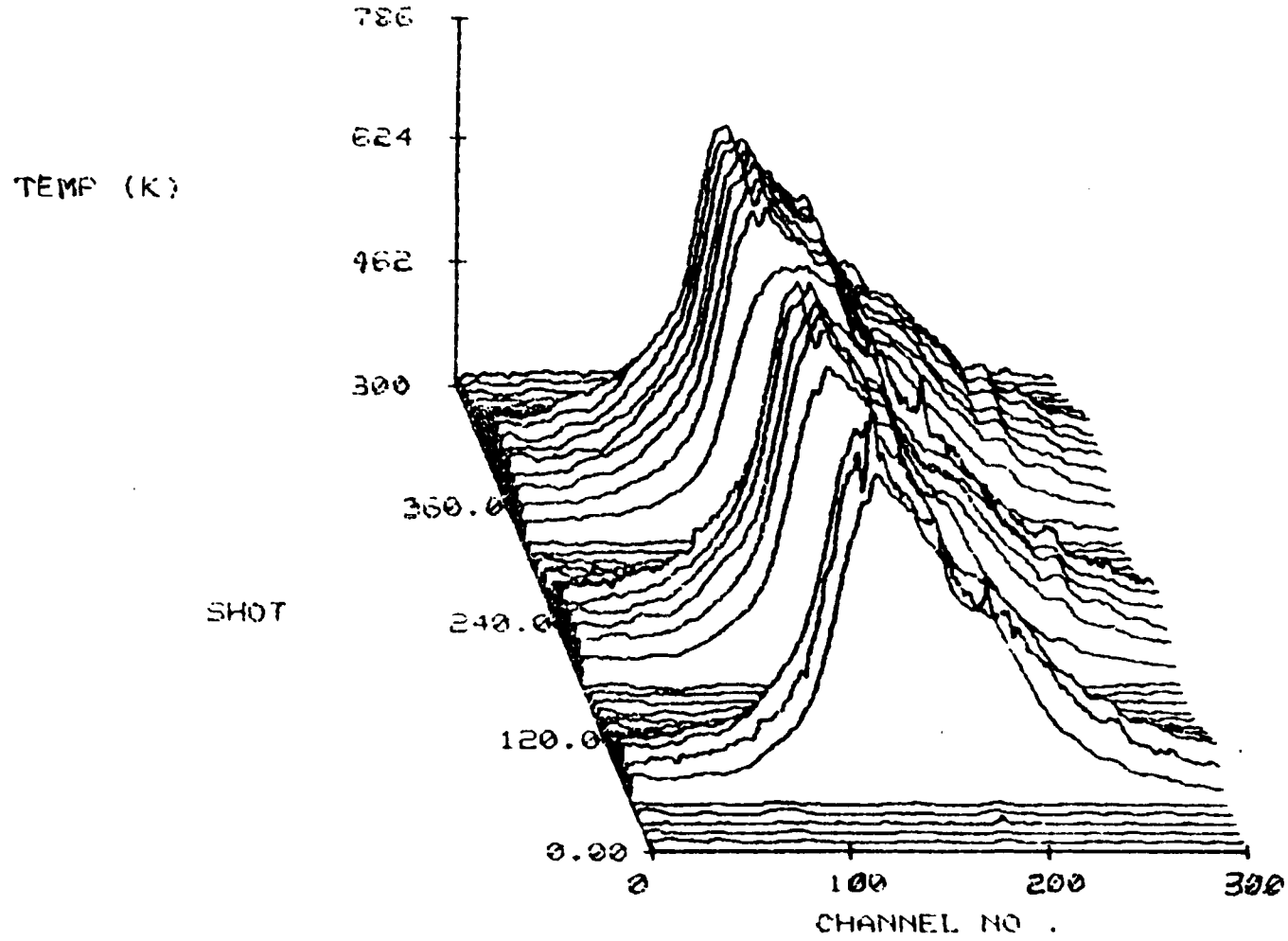

Figure 26. Plot of Three Heating Cycles over 50-second Period for Ceramic Target Heated with CO_2 Laser Focused to ∿ 2 mm Spot.

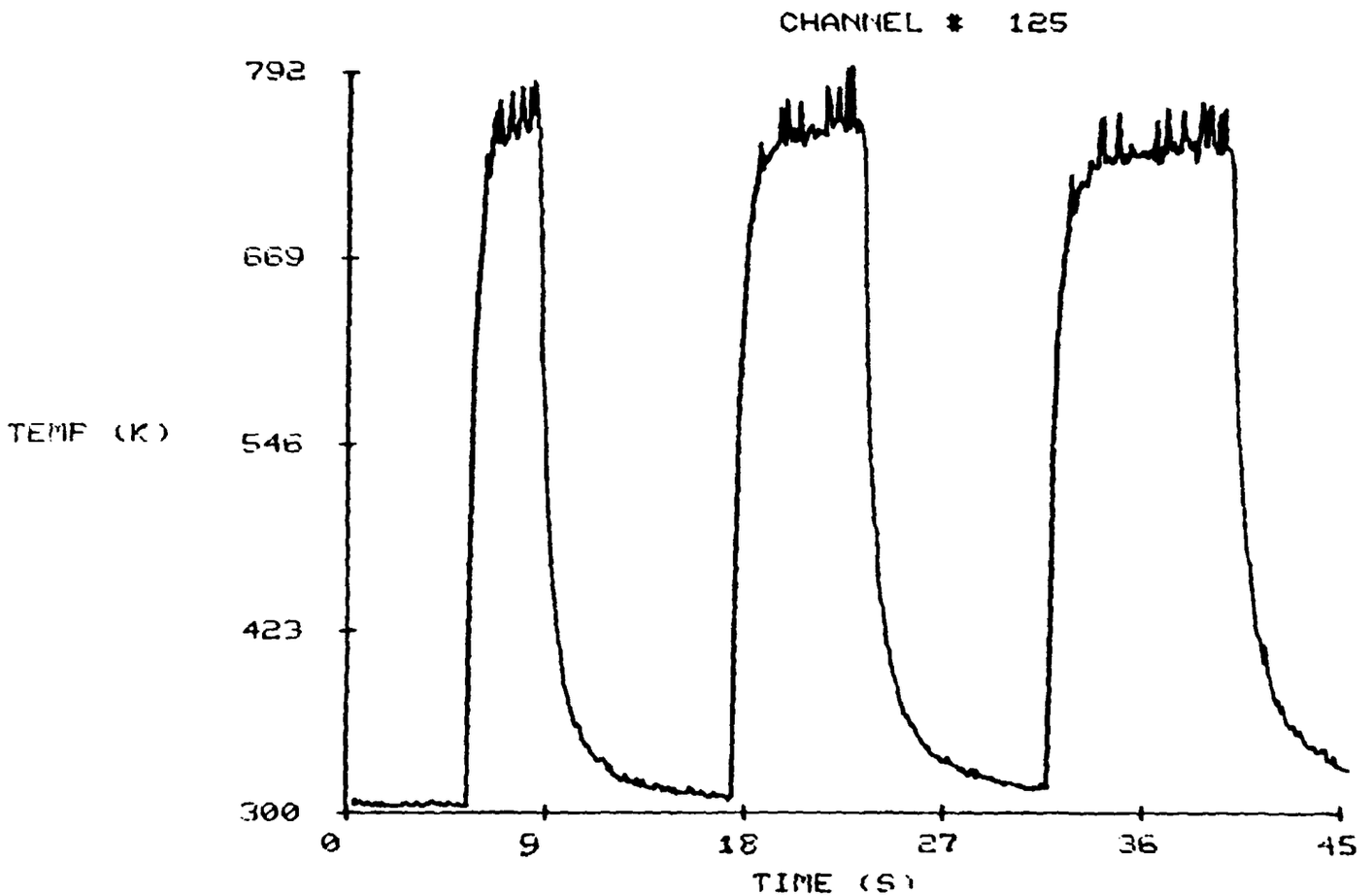

Figure 27. Temporal History of Ceramic Target Heated with CO_2 Laser Focused to ~ 2 mm Spot.

thus, the interdispersed crystals are continuously replenished at the surface. This leads to no observed loss in the fluorescence signal as the surface erodes, and the surface temperature profile can be obtained even on reactive surfaces.

To illustrate this point the experimental configuration displayed in Fig. 22 was utilized on a doped plastic specimen. A 2-mm-focal-spot, 14-W CO_2 beam was used to heat the plastic surface. The experimental setup of the target is illustrated in Fig. 22. The area imaged by the DARSS detector corresponds to 1 cm, which translates into $\sim$ 27.5 μm/channel. As in the case of the ceramic specimen, the CO_2 beam is incident on the sample at an angle of 45 deg.

The excitation of the plastic surface was recorded over two heat-up and cool-down cycles; the results are depicted in Figs. 28 - 30. Under excitation by the CO_2 laser, the plastic surface is actually eroded, as evidenced in Fig. 29 by the increased area over which a high temperature is observed during the second heat-up cycle. As the surface erodes, a hole is formed. The hole increases the surface area covered by the CO_2 excitation beam, resulting in a wider temperature spread during the second heat-up cycle. Figure 31 is a photograph of the plastic surface before and after excitation. A maximum temperature of 560 K was observed for this surface under these conditions.

Note that although the surface was eroding and changing as a function of time, the surface temperature could be easily monitored by this fluorescence technique. Because the plastic actually burned when heated rapidly over a large area, it provided an excellent test case for studying a burning surface to determine whether the imaging system would be adversely affected by sooty flames. Initiation of burning on the surface required that a full non-apertured CO_2 beam of 80 W be incident upon the plastic surface. The resulting flame burned with a strong yellow emission characteristic of heavy soot loading. In this case the temperature distribution across the surface was nearly uniform. This is illustrated in Figs. 32 - 34. Approximately 8 seconds after the initiation of data acquisition, the CO_2 laser was allowed to heat the surface. A very rapid temperature rise was observed which built to $\sim$ 560 K. The

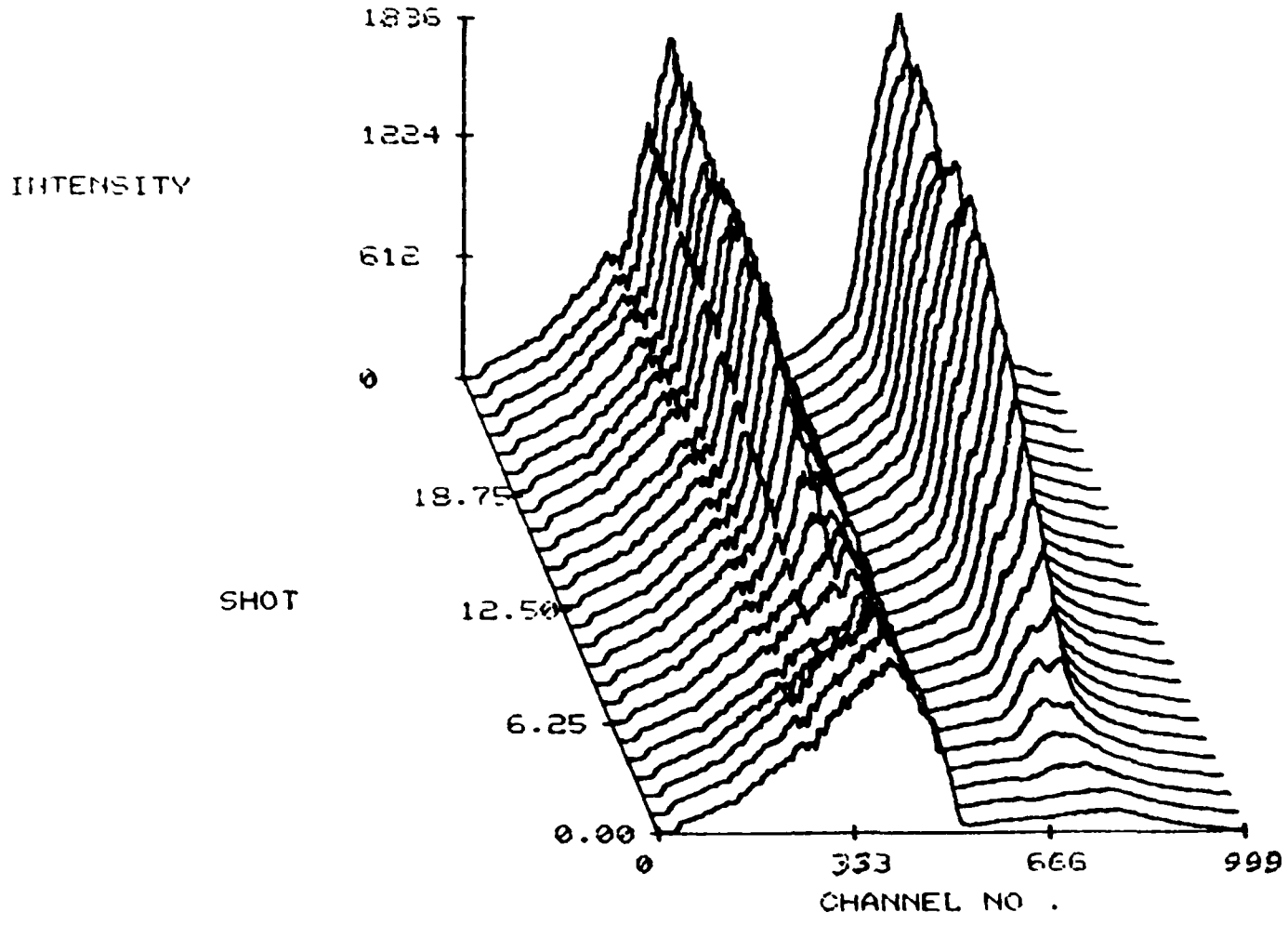

Figure 28. Plot of Fluorescence Intensity of Plastic Target Doped With Dy:YAG Crystals Heated with CO_2 Laser Focused to ~ 2 mm Spot Showing 496- and 467-nm Lines as Observed by DARSS Detector.

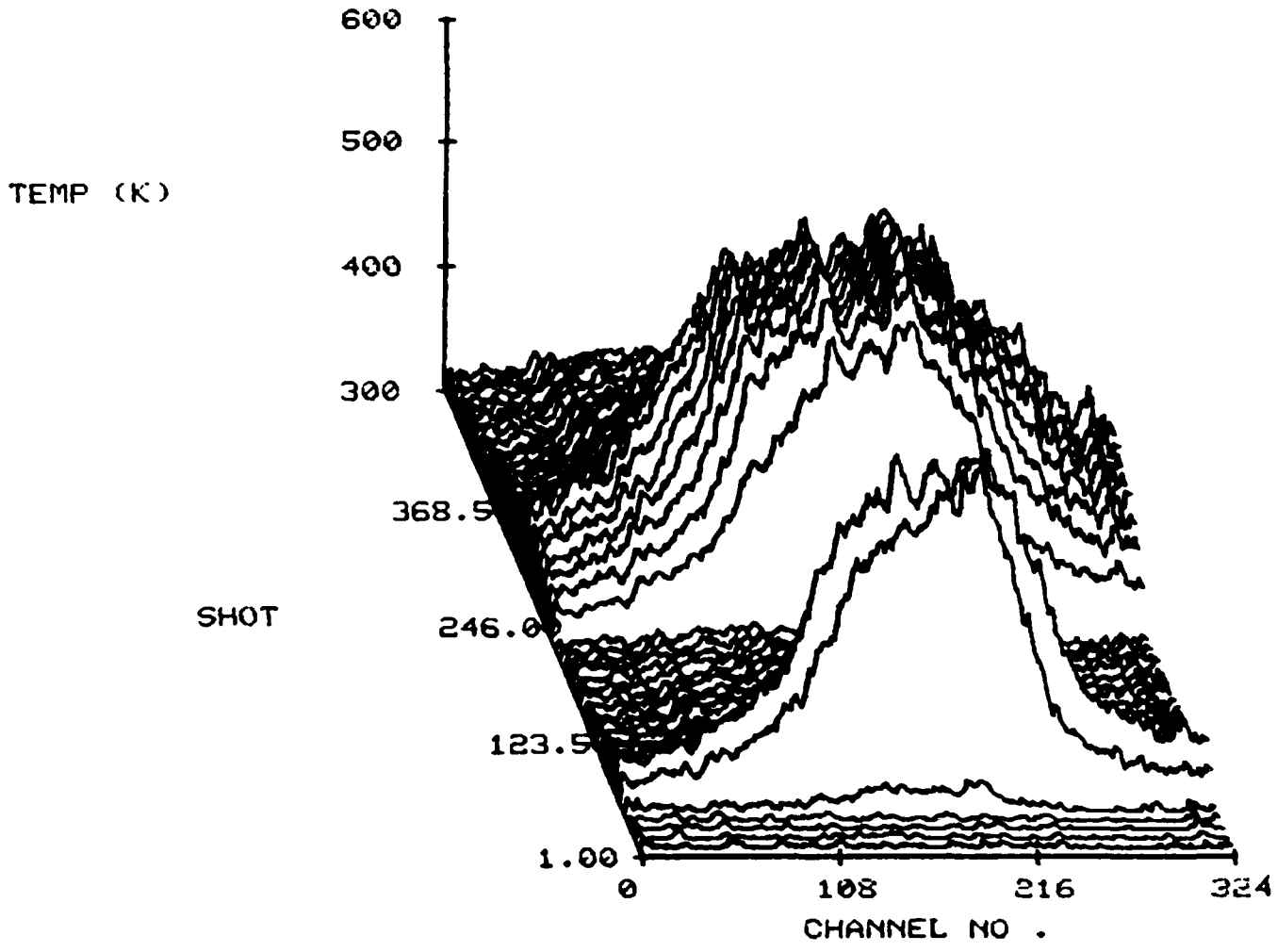

Figure 29. Temperature Plot Resulting from Fig. 28, Two Heating and Cooling Cycles.

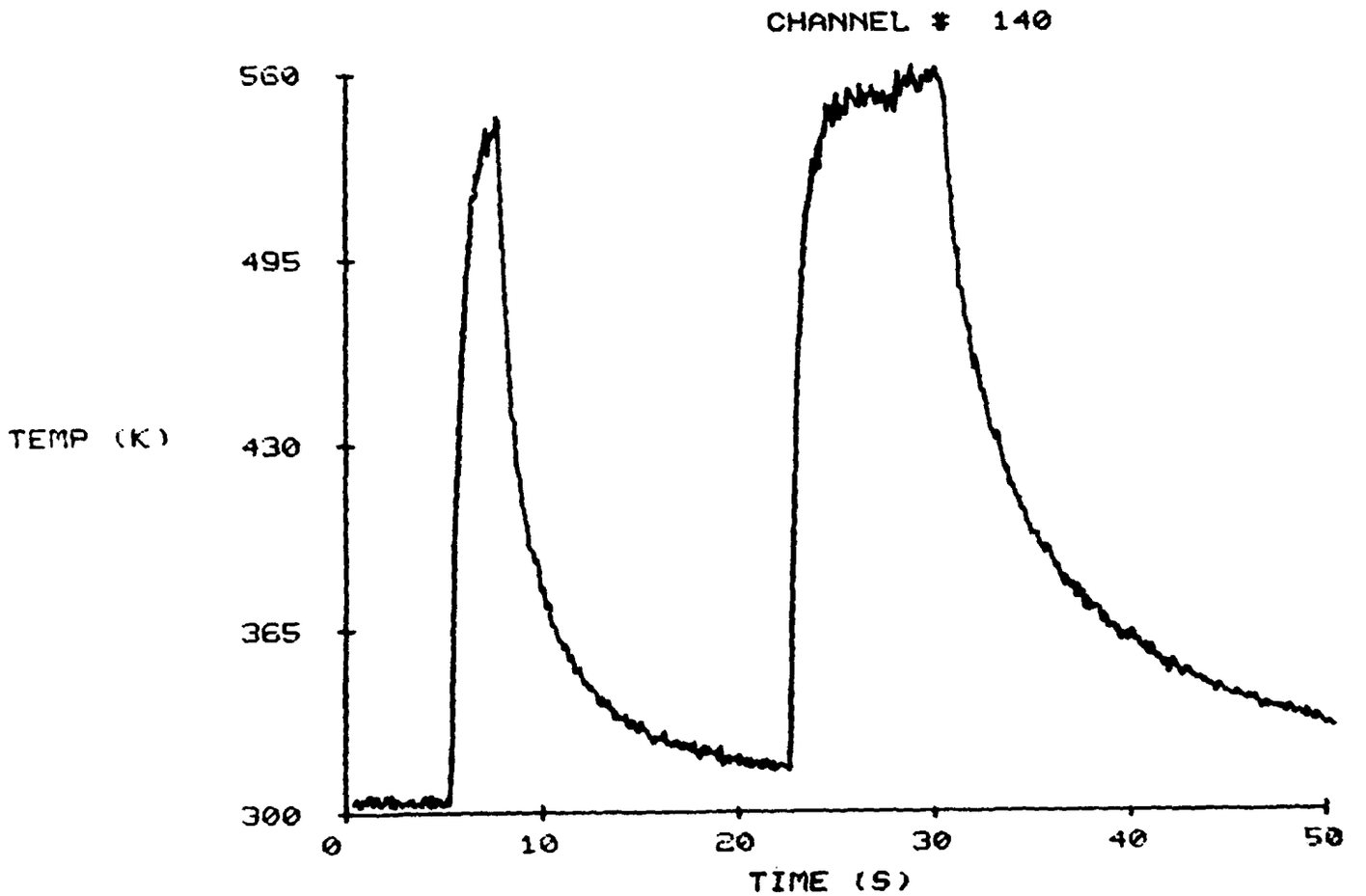

Figure 30. Temporal History of Plastic Target.

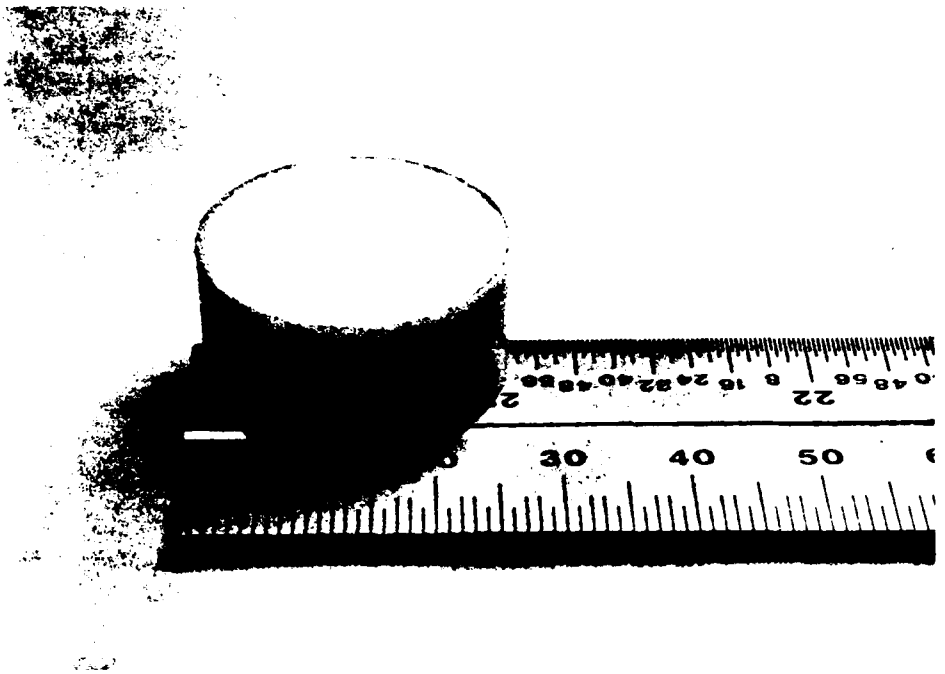

(a)

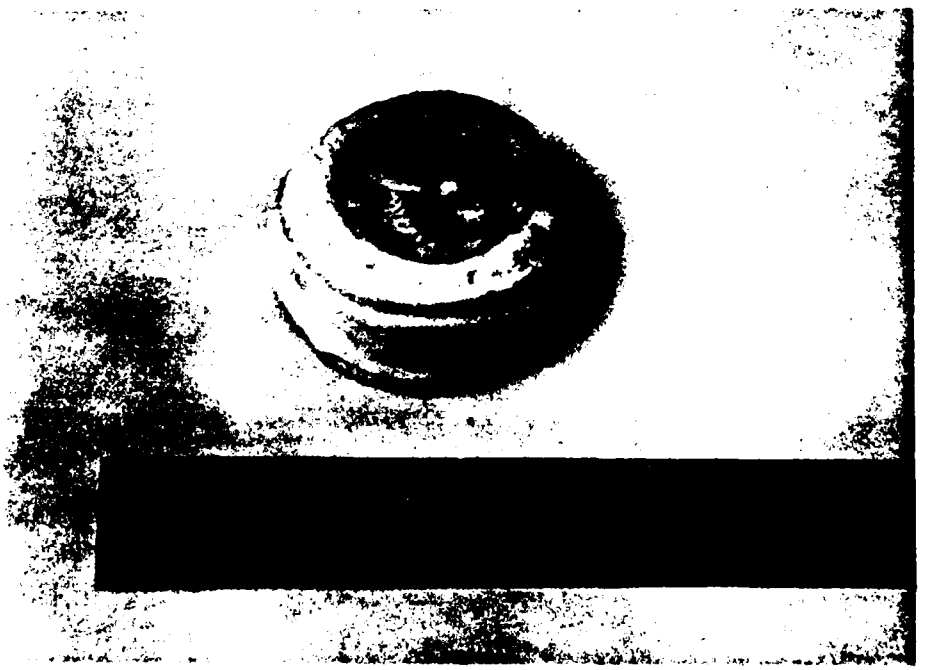

(b)

Figure 31. Photograph of Plastic Surface Before (a) and After (b) Excitation.

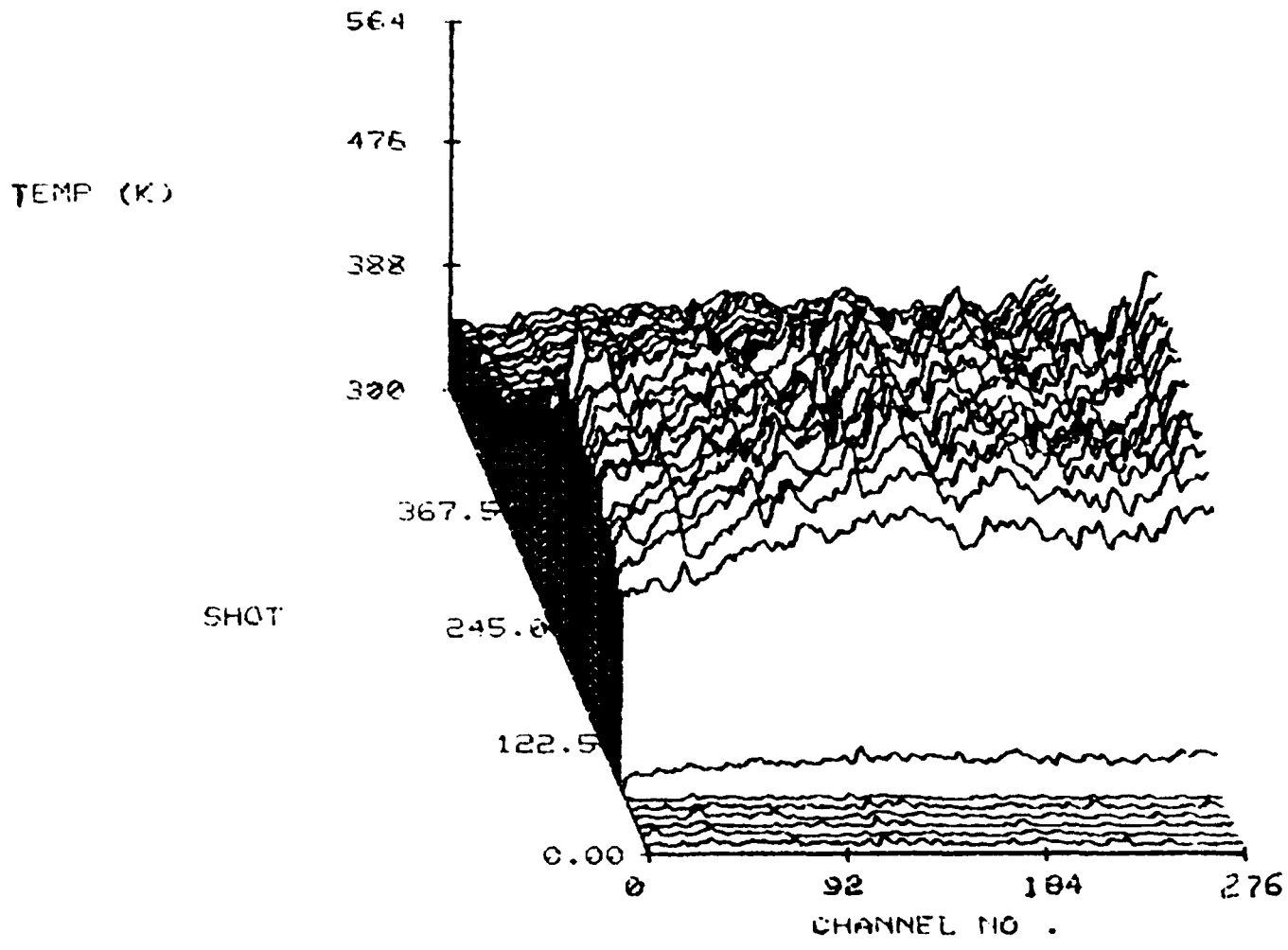

Figure 32. Temperature Plot of Plastic Target Doped with Dy:YAG Crystals Heated over Entire Face with Full-Apertured CO_2 Beam of ~ 2 cm diam., ~ 80 W, One Heating Cycle.

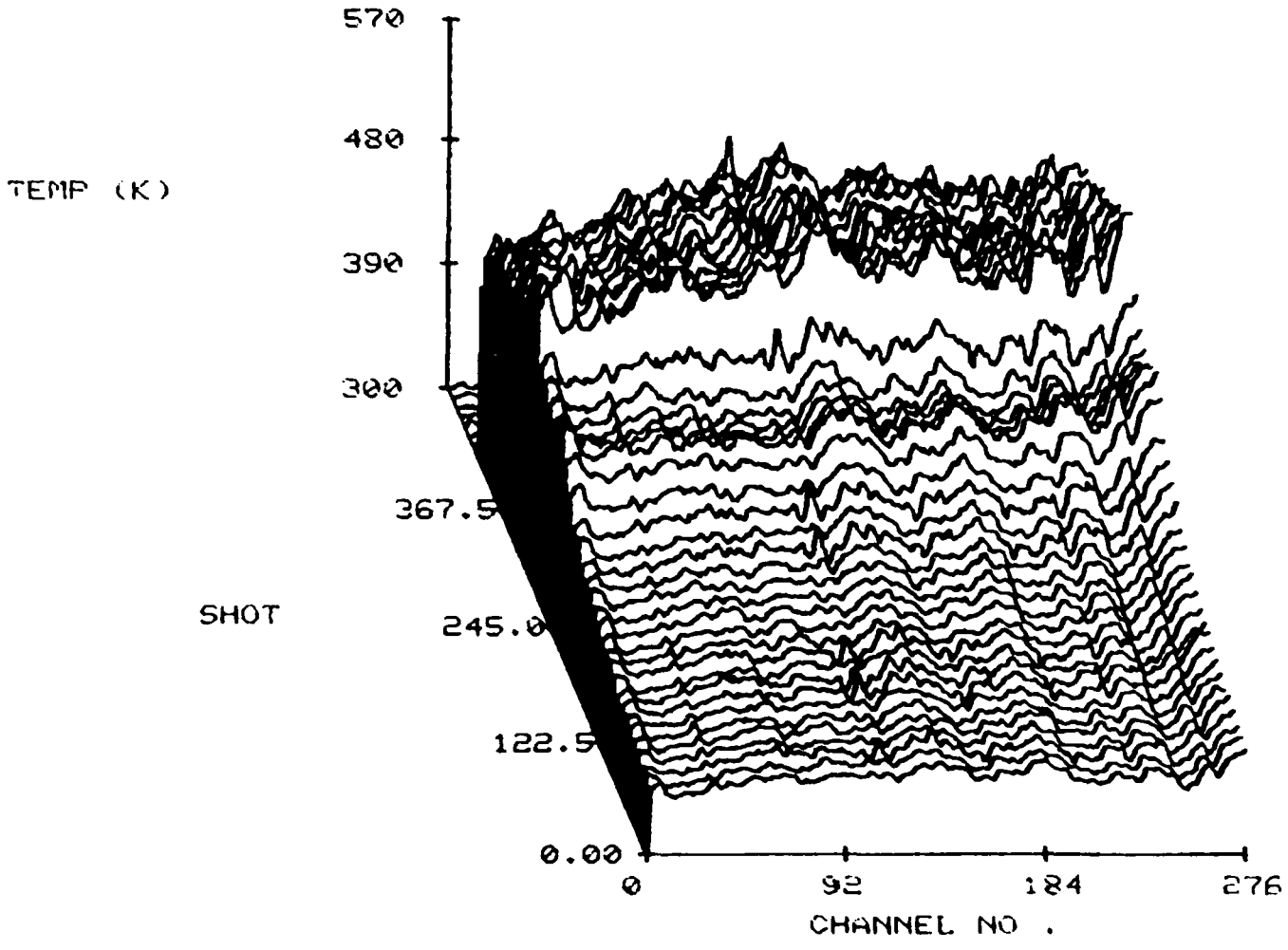

Figure 33. Temperature Plot of Plastic Target Doped with Dy:YAG Crystals Heated over Entire Face with Full-Apertured CO_2 Beam of ∿ 2 cm diam., ∿ 80 W, One Cooling Cycle.

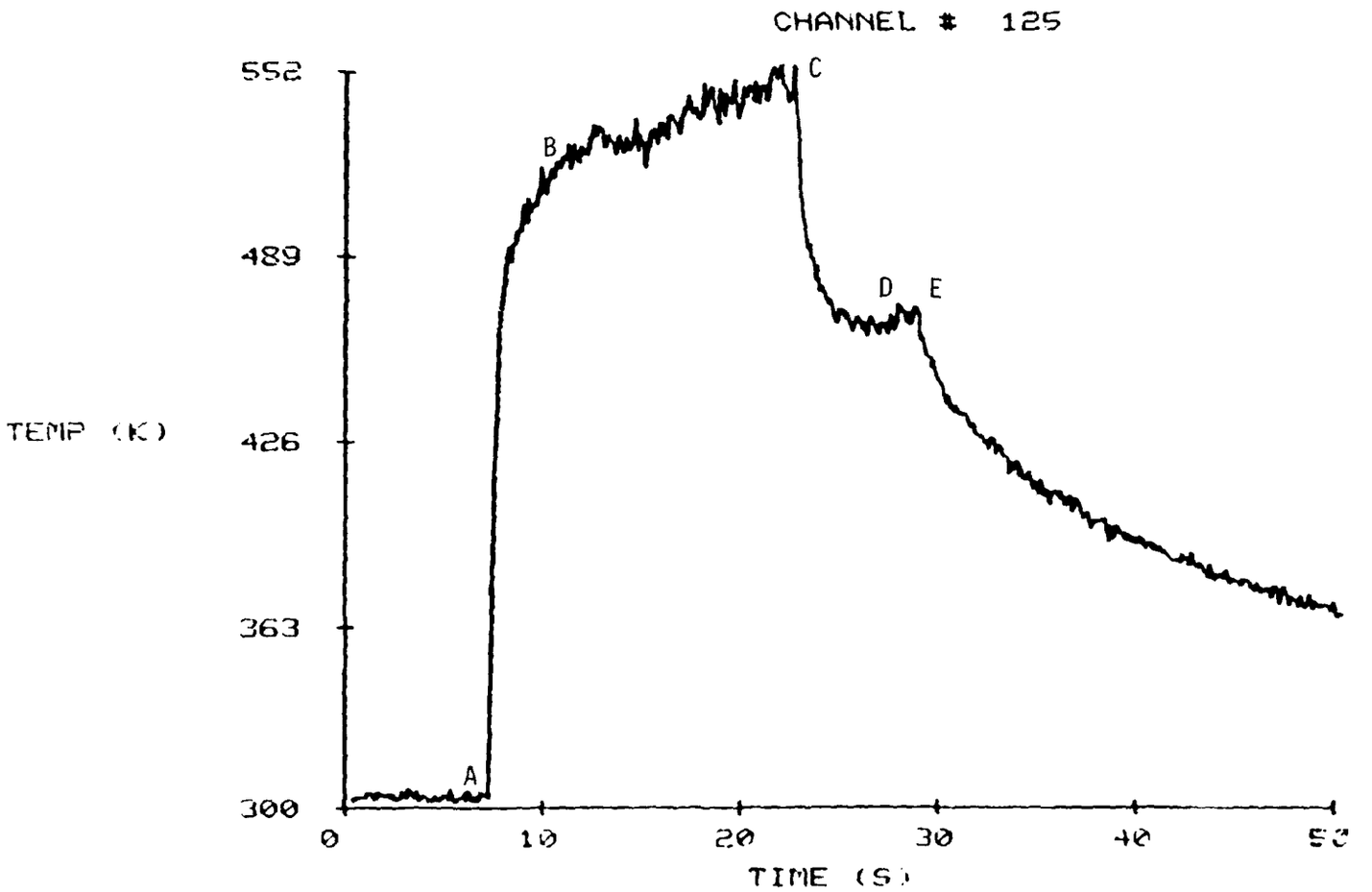

Figure 34. Temperature Plot of Plastic Target Doped with Dy:YAG Crystals Heated over Entire Face with Non-apertured CO_2 Beam of ~ 2 cm Diam., ~ 80 W. A - CO_2 Laser On, B - Target Face Burning, C - CO_2 Laser Off, D - Temperature Due to Active Combustion of Target Material, E - Combustion Extinguished.

excitation was allowed to continue for 16 seconds and was then extinguished. The temperature immediately began to fall, but then rapidly reached a plateau well above room temperature. The temperature of the plateau was ∿ 450 K and was the result of active combustion at the surface. The surface was actively combusting due to the earlier CO_2 excitation. After ∿ 7 seconds the flame was extinguished and the surface temperature decayed in the expected manner.

Note that no interference from the flame was observed nor was any problem denoted by the surface erosion. This clearly illustrates the ability of this technique to function effectively in adverse combustion environments on reactive surfaces.

3.6 Thermal Depth Profiling

Because of the importance of the surface temperature and thermal penetration depth in controlling the reaction rate of energetic materials, an effort was undertaken to apply the LIF technique to the problem of obtaining a temperature depth profile. The classical approach to this measurement involves embedding small thermocouples into the sample and allowing the sample to burn through the thermocouple location. This approach requires the use of small, fragile thermocouples which are destroyed during the measurement process. Problems of determining the exact location of the surface must also be addressed.

One approach which is compatible with the LIF technique involves taking a doped energetic material, trimming the edge to provide a flat surface, and imaging the fluorescence from the side during combustion. This allows the entire depth profile to be monitored as a function of time--two dimensionally rather than at a single point, as demonstrated in Fig. 35. The CO_2 laser is used as the heat source and directed along the edge of the plastic target. The edge is illuminated by the triplet Nd:YAG beam (355 nm) and the fluorescence (temperature) recorded over a period of time. Approximately 30 W of CO_2 power was used to heat the plastic in this study. As the plastic heats and erodes, the CO_2 beam penetrates further along the edge. The temporal history of the temperature profile is monitored while this erosion is taking place. The

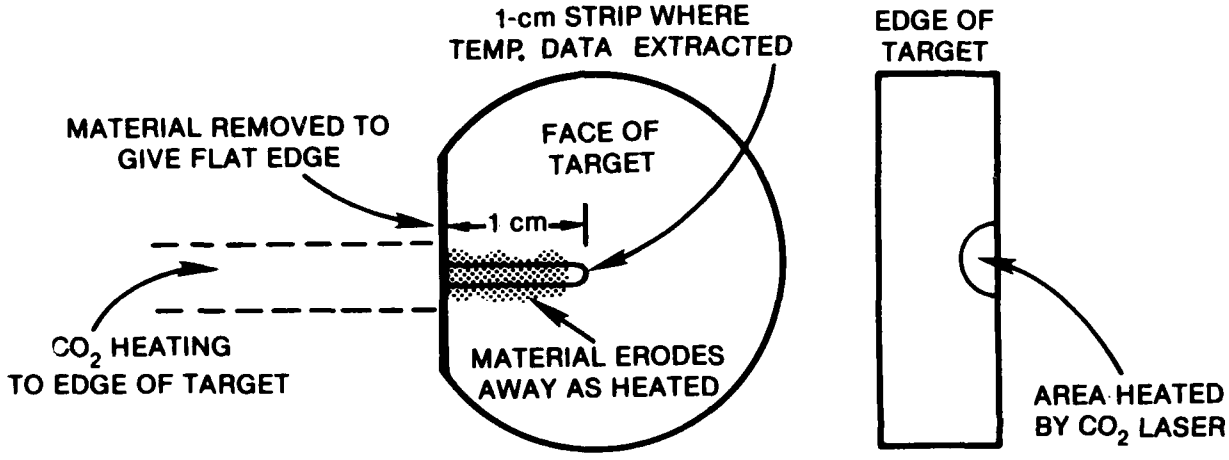

Figure 35. Schematic Diagram of Method for Obtaining Thermal Depth Profile of Energetic Material.

observed thermal depth profile is displayed in Figs. 36 and 37. In Fig. 36 the temperature profile along the edge is displayed at the time intervals indicated. The figure displays the buildup of the surface temperature, the plateau at the maximum surface temperature, and the penetration of the heat into the plastic. Notice that the temperature depth profile which is marked by the dropoff from the maximum temperature plateau is characterized by a steep temperature gradient near the surface followed by a much less steep gradient, displaying temperature penetration quite deep into the surface. The initial temperature drop just beneath the surface is $\sim$ 84 K/mm, which can be observed for $\sim$ 1.54 mm, followed by an $\sim$ 9.8 K/mm drop denoting very deep penetration into the plastic substrate.

The characteristics of the thermal depth profile should be quite sensitive to the frequency of the heat source. A low-frequency source should demonstrate the maximum penetration of the heat into the plastic substrate, while high-frequency temperature fluctuations should remain near the surface with a smaller amount of heat penetration. To test this assumption, the CO_2 laser beam was chopped at 40 and 80 Hz, and the experiment was repeated. The thermal depth profile at 40 Hz is shown in Figs. 38 and 39. The characteristic dual slope is observed in this case; but because of the difference in the frequency of the heat source, the slopes are different. In this case the steep-slope component is $\sim$ 111.1 K/mm, while the second component is $\sim$ 4.67 K/mm. The steep gradient is considerably larger, indicating that the majority of the heat is at the surface and a smaller amount of penetration is occurring at this frequency.

The thermal depth profile at 80 Hz is shown in Figs. 40 and 41. In this case the steep-slope component is $\sim$ 121 K/mm, and the second is 3.4 K/mm. These data further demonstrate that as the frequency of the heat source or wave increases, the thermal wave penetrates to a lesser degree and the thermal depth profile becomes very steep. This appears to be a promising approach which will aid in the understanding of surface thermal processes and how they drive the rate of reaction for energetic materials.

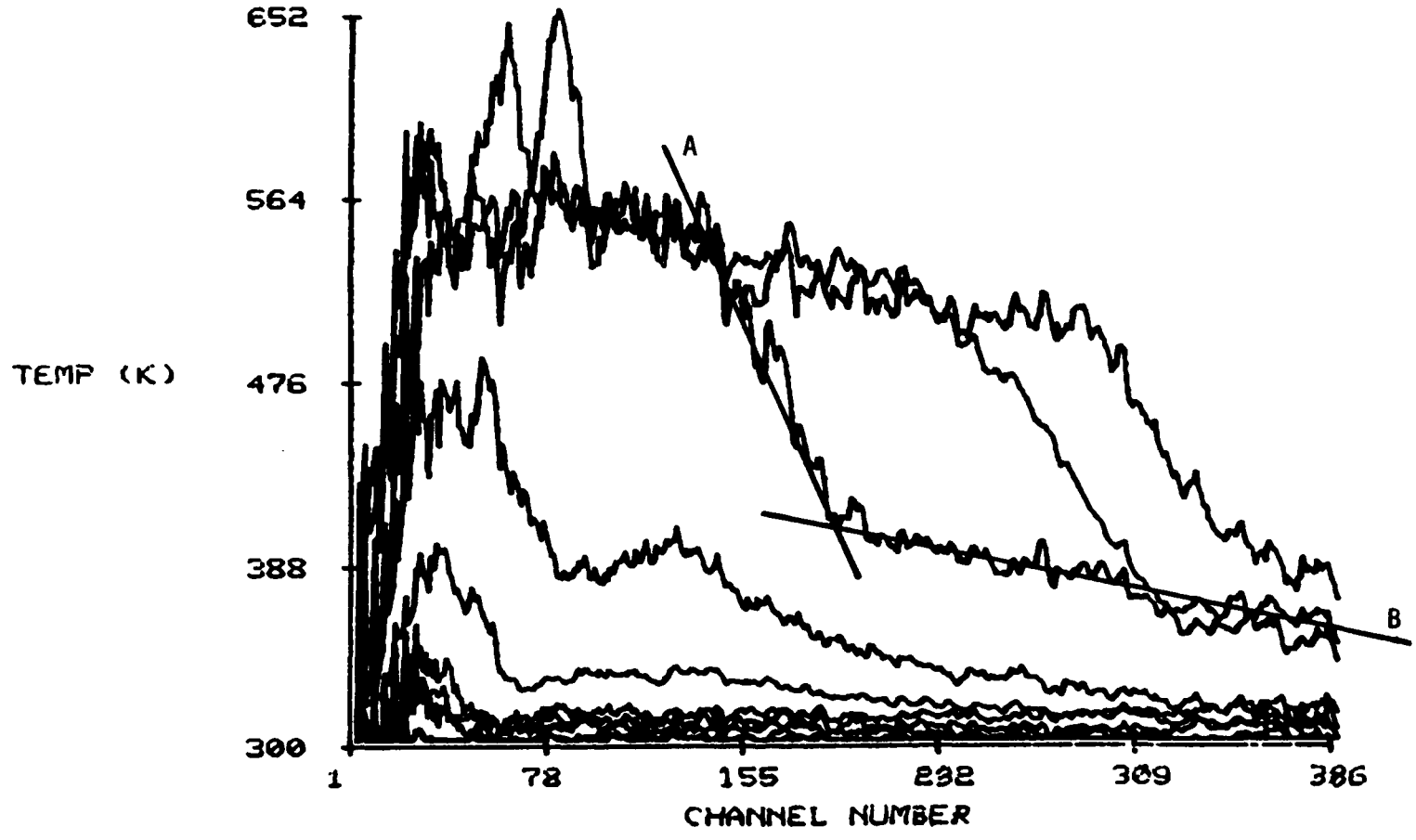

Figure 36. Thermal Depth Profile of Plastic Target Doped with Dy:YAG Heated with CW CO_2 Laser, ~ 30 W.

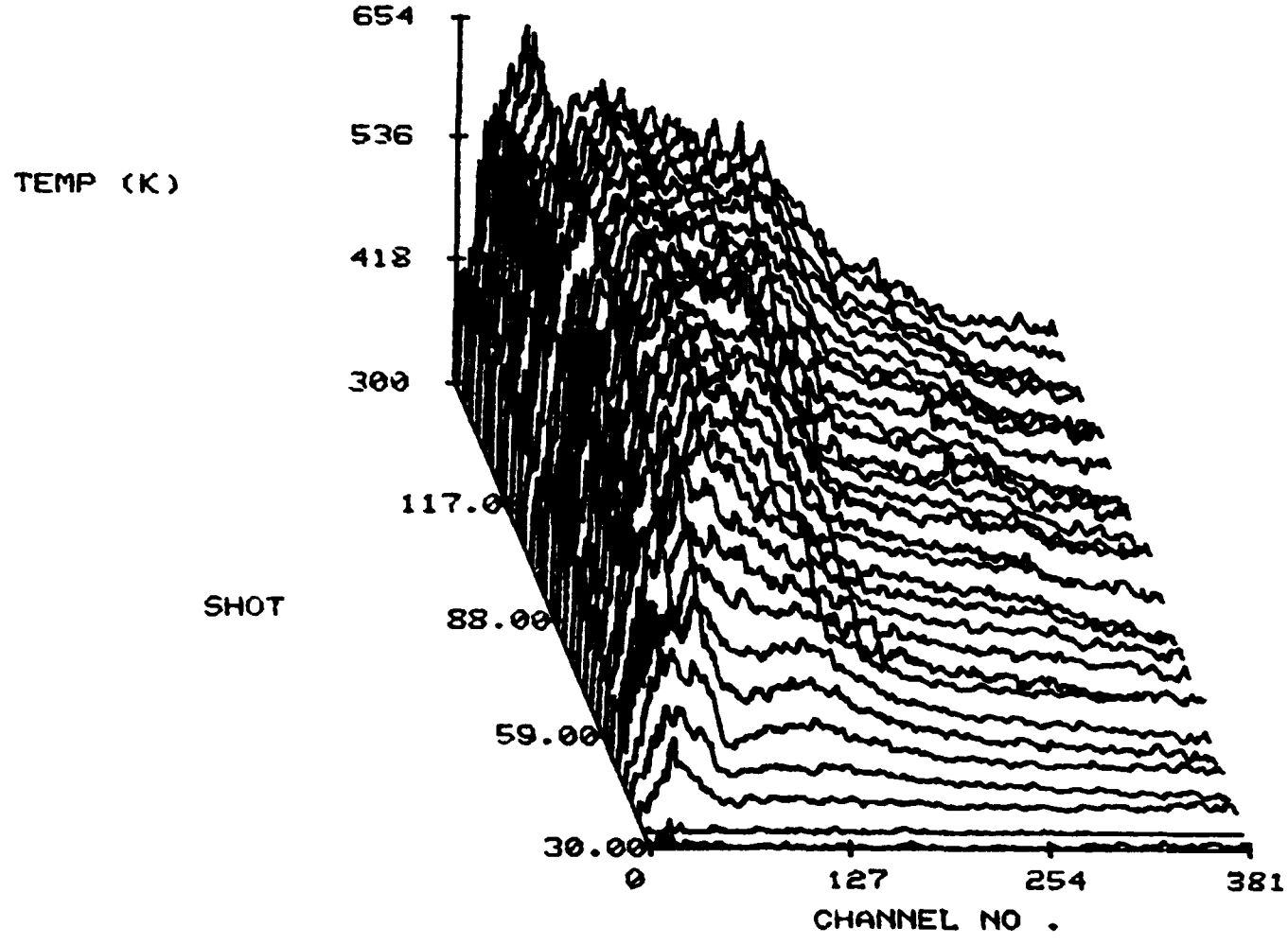

Figure 37. Three-Dimensional Plot of Fig. 36.

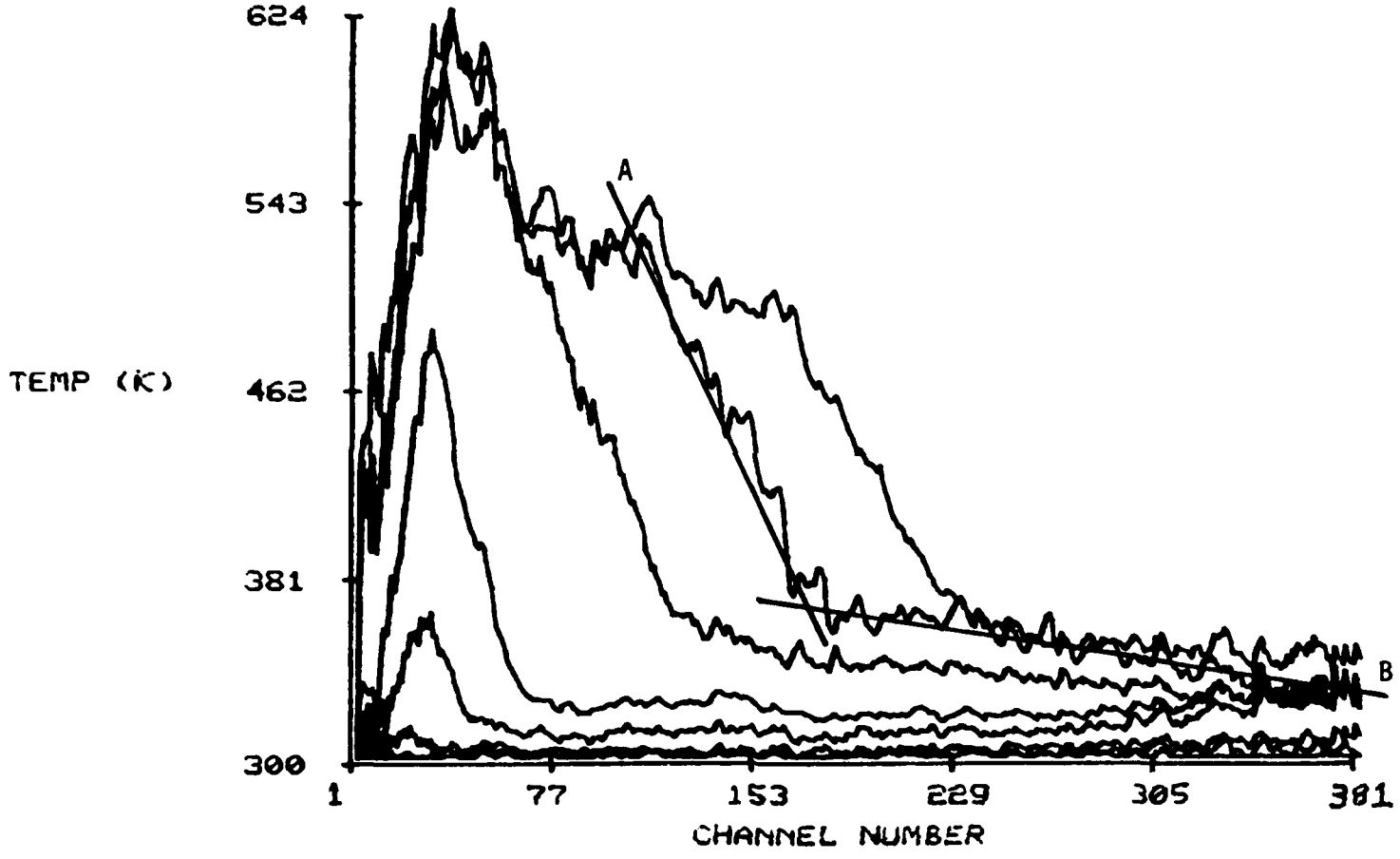

Figure 38. Thermal Depth Profile of Plastic Target Doped With Dy:YAG.

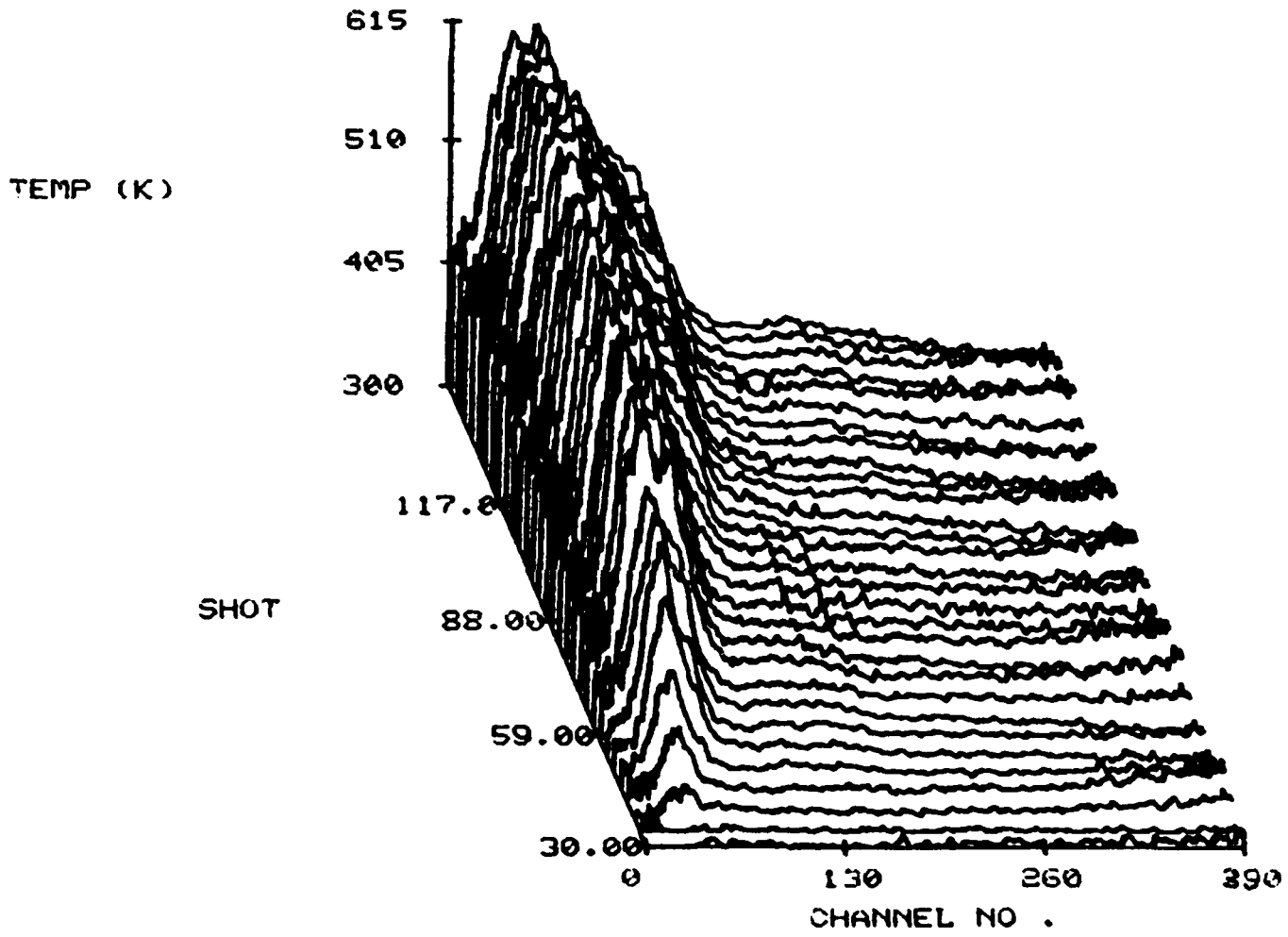

Figure 39. Three-Dimentional Plot of Fig. 38.

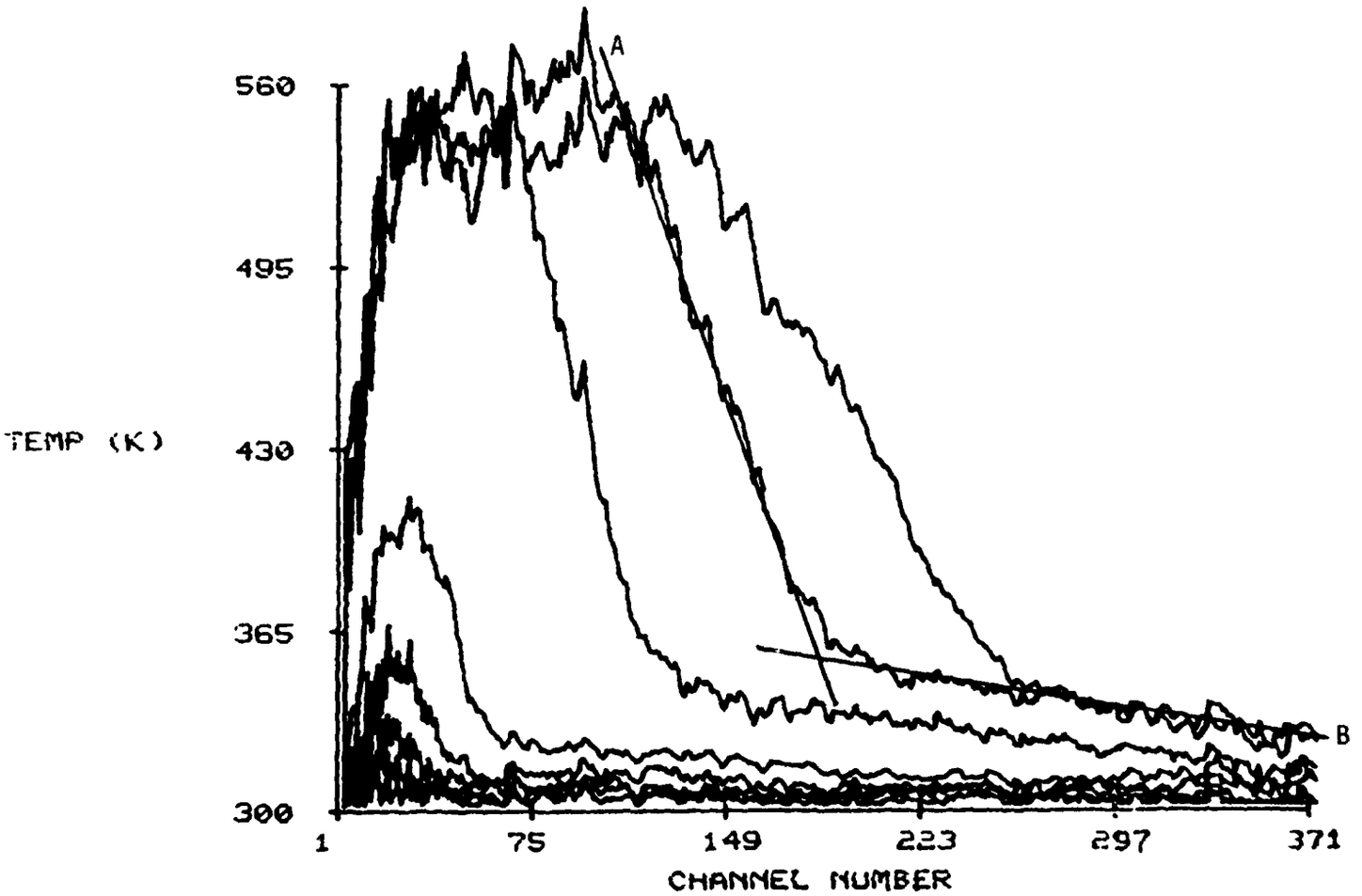

Figure 40. Thermal Depth Profile of Plastic Target Doped with Dy:YAG Heated With Pulsed 40-Hz CO_2 Laser, ~ 30 W.

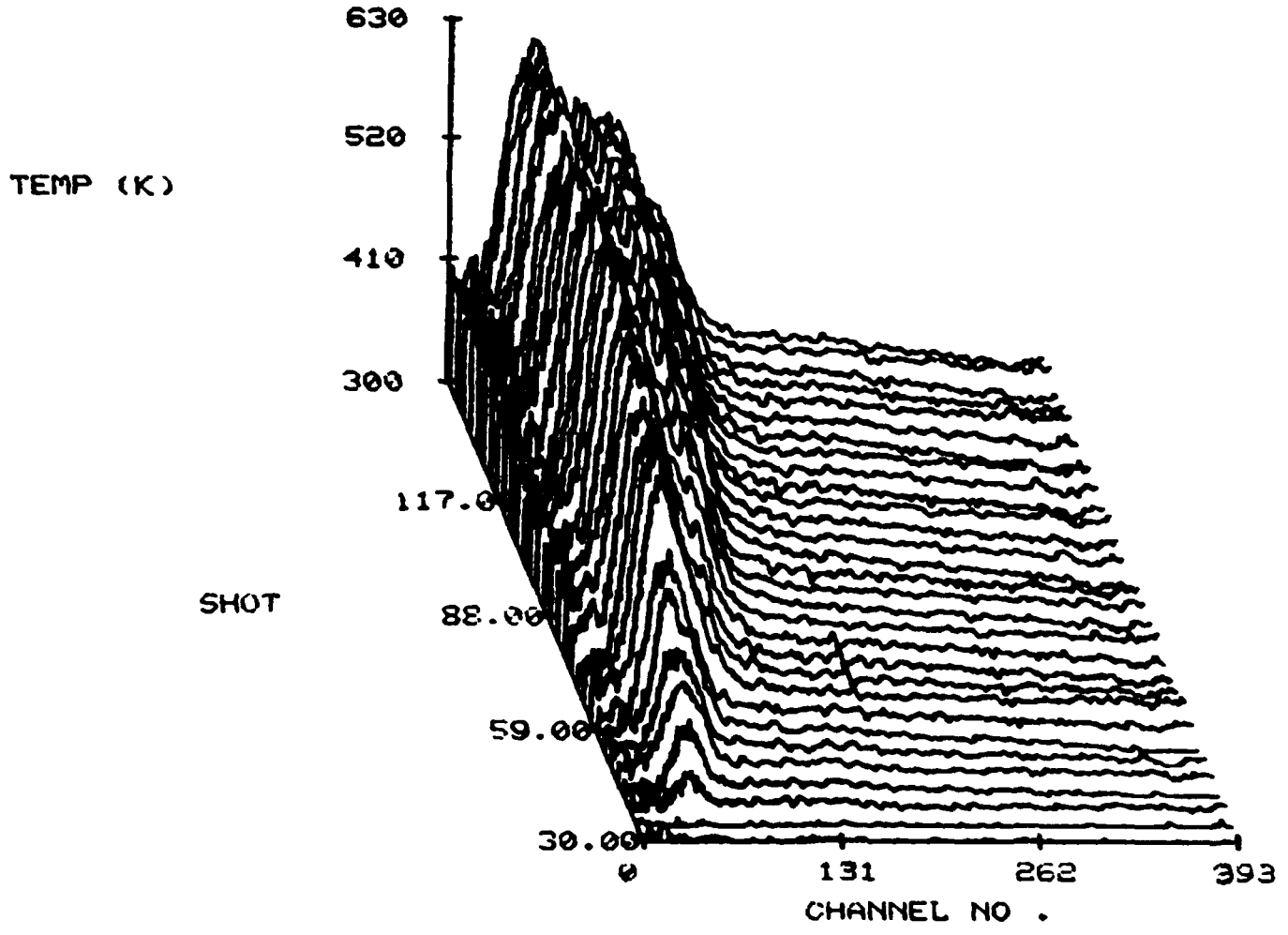

Figure 41. Three-Dimensional Plot of Fig. 40.

Section 4

CONCLUSIONS

In conclusion, the three primary objectives--selecting a dopant species, calibrating its temperature response, and applying it to the study of nonreacting and reacting surfaces under rapid CO_2 laser heating--have been demonstrated. The selection of the LIF technique for this work has led to the extension of point measurements to line measurements and, with the use of two-dimensional camera systems, possibly to full-surface temperature profiling. The technique also lends itself to the measurement of temperature depth profiles which are very important in understanding the reaction rates of energetic materials.

Section 5

PRESENTATIONS DURING THIS REPORTING PERIOD

The following presentations were made during this reporting period:

"Application of Fluorescence to Measurement of Surface Temperature in Solid Propellants" (L. P. Goss and A. A. Smith), Presented at the 21st JANNAF Combustion Meeting, October 1-5, 1984, Laurel, Maryland. Published in conference proceedings.

"Application of Laser-Induced Fluorescence to Measurement of Surface Temperature in Solid Propellants" (A. A. Smith and L. P. Goss), Presented at the International Conference on Lasers '84, November 26-30, 1984, San Francisco, California. Abstract published.

"Application of Fluorescence to Measurement of Surface Temperature" (L. P. Goss and A. A. Smith), Poster Presentation at the Seventh International Conference on Laser Spectroscopy, June 24-28, 1985, Maui, Hawaii. Abstract published.

"Measurement of Surface Temperature by Laser-Induced Fluorescence" (L. P. Goss, A. A. Smith, and R. A. Olson), Invited Presentation at the Gordon Research Conference on Physics and Chemistry of Laser Diagnostics in Combustion, July 15-19, 1985, New London, New Hampshire.

"Application of Fluorescence to Measurement of Surface Temperature in Solid Propellants" (L. P. Goss and A. A. Smith) Invited Presentation at the Workshop on Combustion Probes for Solid Nitramines, June 9-11, 1986, Sandia National Laboratories, Livermore, California.

"Application of Fluorescence to Measurement of Surface Temperature in Solid Propellants" (L. P. Goss and A. A. Smith), Presented at the 1986 AFOSR Contractors Meeting on Diagnostics of Reacting Flows, June 16-17, 1986, Stanford, California. Published in conference proceedings.

REFERENCES

1. Fundamentals of Solid-Propellant Combustion, Vol. 90 in Progress in Astronautics and Aeronautics (K. K. Kuo and M. Summerfield, eds.) (American Institute of Aeronautics and Astronautics, Inc., New York, 1984).

2. L. P. Goss and A. A. Smith, "Application of Laser-Induced Fluorescence to Measurement of Surface Temperature in Solid Propellants," Presented at the 21st JANNAF Combustion Meeting held October 1 - 5, 1984, in Laurel, Maryland.

END

5-87

DTIC